



**Politecnico
di Torino**

Politecnico di Torino

Master's Degree in Automotive Engineering

Accademic Year 2022/2023

October 2023

Master's Degree Thesis

Validation of CFD model in Wind Tunnel and study of Aerodynamic Maps

Supervisors

Prof. Andrea Tonoli

Ing. Giuseppe Scantamburlo

Candidate

Lorenzo Borgialli

Abstract

This thesis presents a comprehensive study focused on the validation of a Computational Fluid Dynamics (CFD) model for a Formula SAE (Society of Automotive Engineers) car within the controlled environment of the Stellantis Wind Tunnel. Additionally, the research endeavors to develop a linear model of aerodynamic maps that accounts for the car's cornering condition. The research utilizes a combination of software tools, including CATIA for design, BETA CAE Systems for geometry preparation, and STAR-CCM+ for both pre-processing and post-processing of the CFD simulations.

The primary objective of this research is to assess the accuracy and reliability of the CFD model in replicating the aerodynamic behavior of the Formula SAE car when subjected to real-world wind conditions. To achieve this, a series of wind tunnel tests are conducted, generating empirical data that serves as a benchmark for validating the CFD model. The thesis systematically compares the CFD simulations with wind tunnel measurements, with a focus on key aerodynamic parameters such as drag and downforce.

Furthermore, the study extends its scope to address the unique aerodynamic challenges posed by the car's cornering conditions. A linear model is developed to predict how changes in vehicle orientation and steering angles impact the car's aerodynamic performance. This model is derived from the CFD simulations and empirical data, providing valuable insights into the car's behavior during dynamic maneuvers.

The results obtained from this research have implications for improving the overall performance and stability of Formula SAE cars during competitions. By establishing the accuracy of the CFD model and creating a linear aerodynamic model that accounts for cornering conditions, this thesis contributes to the advancement of Formula SAE vehicle design and optimization. Additionally, the methodology and tools used in this research can be adapted for similar studies in the field of automotive aerodynamics, furthering our understanding of vehicle performance in various conditions.

Acknowledgements

Giunto alla fine di questo percorso, desidero ringraziare tutte le persone che mi sono state vicine in questi anni. Inizialmente vorrei ringraziare il Professor Tonoli, tutore del team Squadra Corse e relatore di questa tesi, per la sua guida e il suo supporto.

Desidero inoltre ringraziare i colleghi di Squadra Corse, con i quali ho passato due anni bellissimi della mia vita e ho condiviso momenti che mi porterò dietro per sempre.

Un ringraziamento speciale va alla mia famiglia che mi ha sempre sostenuto, qualsiasi cosa decidessi di fare. Grazie a mia mamma che è sempre la prima persona a credere in me e nonostante questo ultimo brutto periodo mi ha insegnato ad essere comunque positivo. Grazie a mio papà perchè è stato un esempio e una figura modello, spero di averti reso fiero di ciò che sono. Grazie ai miei fratelli Icca e Nannu perchè senza di loro non sarei riuscito a fare nemmeno la metà delle cose che ho fatto.

Un grazie va ai miei nonni Marcello e Marisa che mi sono stati vicino e aiutato, soprattutto in questo percorso di vita. Grazie anche alla mia nonna Chiara che ormai non c'è più ma che sicuro da lassù si starà vantando del suo nipote ingegnere. Un grazie a tutti i miei amici senza i quali non sarei il tipo di persona che sono, mi avete fatto crescere tantissimo e sapere di poter sempre contare su di voi mi fa capire di essere veramente fortunato.

Vorrei dedicare un momento speciale per ringraziare la persona che ha svolto un ruolo cruciale nella mia vita durante il mio percorso di studio e nella realizzazione di questa tesi di laurea. La mia fidanzata, Chiara. Grazie, per la tua pazienza infinita, la tua comprensione e il tuo sostegno incondizionato. Sono incredibilmente fortunato ad averti nella mia vita, e non vedo l'ora di condividere ancora molti successi futuri con te.

Per finire voglio dire un grazie a mio nonno Lorenzo che senza volerlo mi ha spinto sin da piccolo a intraprendere questo percorso e senza il quale non avrei capito tanti valori della vita. Questo traguardo è dedicato a te nonno. Ora potrai dire ancora una volta *bravo, sette +*.



Table of Contents

List of Tables	VI
List of Figures	VII
Acronyms	X
1 Introduction	1
1.1 Formula Student	1
1.2 Aerodynamics & CFD Division	3
1.3 Background and Motivation	4
1.4 Research Objectives	5
2 Literature Review	7
2.1 Overview of CFD Modeling	7
2.1.1 Governing Equation	7
2.1.2 Discretization Methods	11
2.1.3 Turbulence Models	13
3 Methodology	17
3.1 Geometry and Mesh Generation	18
3.2 Boundary and Initial Conditions	23
3.3 Numerical Methods	27
4 Validation Case	29
4.1 Experimental Data	30
4.2 Flow Phenomenon	33
5 Results and Discussion	36
5.1 Data Analysis	36
5.2 Sources of Discrepancy	48

6	Aerodynamic Maps and Cornering Simulations	51
6.1	Ride Height Aero Map	51
6.2	Skidpad Cornering Simulation	55
6.2.1	Simulation setup	57
6.3	Derivatives of Aerodynamic Coefficients	59
6.4	Yaw rate Simulation	61
6.5	Beta Simulation	64
6.6	Results	66
7	Conclusion and Future Work	68
7.1	Summary of Findings	68
7.2	Future Recommendations	70
	Bibliography	71

List of Tables

3.1	Mesh refinement	20
3.2	Porous Media	25
3.3	Fans Modelling Results	26
5.1	Aerodynamics Coefficient 60kph	37
5.2	Delta Aerodynamics Coefficient 60kph	37
5.3	Aerodynamics Balance 60kph	37
5.4	Aerodynamics Coefficient and Delta 40kph	38
5.5	Aerodynamics Balance 40kph	39
5.6	Aerodynamics Coefficient and Delta 80kph	39
5.7	Aerodynamics Balance 80kph	39
5.8	Aerodynamics Coefficient and Delta 100kph	39
5.9	Aerodynamics Balance 100kph	39
6.1	Definition of sketches for the refinement boxes [9]	58
6.2	Yaw rate Table Coefficient	62
6.3	Sideslip Table Coefficient	64
6.4	Sideforce Aerodynamics Coefficient Derivatives	66
6.5	Yaw Moment Aerodynamics Coefficient Derivatives	66
6.6	Comparison of CFD and Linear Model	67

List of Figures

1.1	Formula Student Germany 2023 Panoramic Picture	2
1.2	Total Pressure Coefficient + Streamlines SC23	3
1.3	Aeropack SC22	4
2.1	Classification of Cell Type [3]	12
2.2	Turbulence Model - RANS [4]	15
2.3	Instantaneous Velocity	16
3.1	SC22 - Varano	17
3.2	SC23 - CATIA	18
3.3	Domain - BETA CAE ANSA	19
3.4	Detail of MRF zone (green) with polyhedral mesh	20
3.5	Example of Box Refinements (Wings)	20
3.6	Inner Layer	22
3.7	Low y^+	22
3.8	High y^+	23
3.9	Turbulent Viscosity Ratio	23
3.10	Fans Modelling	25
3.11	Fan Curve STAR-CCM+	27
4.1	Team in FCA wind tunnel	30
4.2	Car fitting to the Rolling Road Simulation System	31
4.3	Pressure taps on the rear wing	32
4.4	Wake measurement system	33
4.5	Test section in the CFD Model	33
4.6	Car setup	34
4.7	y^+ in Wind Tunnel CFD Simulation	35
5.1	Pressure Coefficient on Rear Wing, $Y=306$ mmm	41
5.2	Wake measurement 1	42
5.3	Wake measurement 2	42
5.4	Wake measurement 3	43

5.5	Wake measurement 4	43
5.6	Wake measurement 5	44
5.7	Wake measurement 6	44
5.8	Wake measurement 7	44
5.9	Wake measurement 8	45
5.10	Wake measurement 9	45
5.11	Wake measurement 10	46
5.12	Wake measurement 11	46
5.13	Wake measurement 12	47
5.14	Wake measurement 13	47
6.1	Geometry Setup	52
6.2	DFM Function ANSA	53
6.3	Ride Height Table	53
6.4	AeroMap C_x	54
6.5	AeroMap C_z	54
6.6	AeroMap Aerobalance	55
6.7	Side Slip Angle definition	56
6.8	Construction of the Skidpad domain	57
6.9	Refinement Boxes [9]	58
6.10	Scheme of Boundary Conditions	59
6.11	Y_r	62
6.12	N_r	63
6.13	Sideslip Simulation - Top View	64
6.14	Y_β	65
6.15	N_β	66

Acronyms

CFD

Computational Fluid Dynamics

SC

Squadra Corse

CAD

Computer-Aided Design

FDM

Finite Difference Method

FVM

Finite Volume Method

FEM

Finite Element Method

RANS

Reynolds-Averaged Navier-Stokes

RSM

Reynolds Stress Mode

LES

Large Eddy Simulation

DNS

Direct Numerical Simulation

MRF

Multiple Reference Frames

WSU

Wheel Spinning Unit

Chapter 1

Introduction

1.1 Formula Student

Formula Student is an international engineering competition for university students that challenges teams to design, build, and race formula-style race cars. Organized by the Institution of Mechanical Engineers (IMechE) and the Society of Automotive Engineers (SAE), Formula Student competitions take place in various regions around the world, including Europe, North America, Asia, and more. The competition encompasses various aspects of engineering, including mechanical design, aerodynamics, electronics, and overall vehicle performance optimization.

Participating in Formula Student offers students a unique opportunity to bridge the gap between theoretical knowledge gained in classrooms and practical engineering experience. It also nurtures skills such as teamwork, communication, project management, and entrepreneurship, which are invaluable for their future careers in the engineering and automotive industries.

Moreover, Formula Student is a great platform for networking and showcasing talent to potential employers and industry professionals, as many companies in the automotive and motorsport sectors are closely involved with the competition. Overall, it's an exceptional way for students to apply their academic learning in a hands-on, competitive environment while gaining skills that extend beyond the realm of engineering.

The competition typically involves the following key elements:

- **Design and Build:** Participating teams are required to design and manufacture a small, open-wheel, formula-style race car from scratch. This includes developing the vehicle's chassis, suspension, powertrain, aerodynamics, and other components. The design should be innovative, practical, and tailored to perform well in various dynamic events.



Figure 1.1: Formula Student Germany 2023 Panoramic Picture [1]

- **Static Events:** These events assess the team's ability to present and defend their design and business case. They include:
 - **Design Presentation:** Teams present their engineering design and development processes to a panel of judges, explaining the rationale behind their decisions.
 - **Cost Analysis:** Teams create a budget and justify the costs associated with manufacturing and operating their vehicle.
 - **Business Presentation:** Teams pitch their vehicle as a marketable product, showcasing their marketing, sales, and financial strategies.
- **Dynamic Events:** These events test the car's performance and handling capabilities:
 - **Acceleration:** The car's acceleration from a standstill over a short distance is measured.
 - **Skid Pad:** The car navigates a figure-eight course to assess its lateral grip and handling
 - **Autocross:** The car completes a timed obstacle course to showcase its agility, acceleration, and overall handling.

- **Endurance & Efficiency:** the endurance event evaluates the car's durability and reliability by testing its performance over a long distance race, the track has the same characteristics of the Autocross one and the total event is around 22 km long. After the course is completed, the total energy consumption, taking into account also the regenerated amount as a negative contribution, is calculated and so the efficiency event leader board is established.

The future of Formula Student is promising, as the competition continues to evolve and adapt to the changing landscape of motorsport and mobility. The competition is expected to embrace new technologies, such as autonomous driving, electric and hybrid powertrains, and advanced materials and manufacturing methods. Overall, Formula Student is an exciting and rewarding program that offers students a unique and valuable experience in the world of engineering and motorsport.

1.2 Aerodynamics & CFD Division

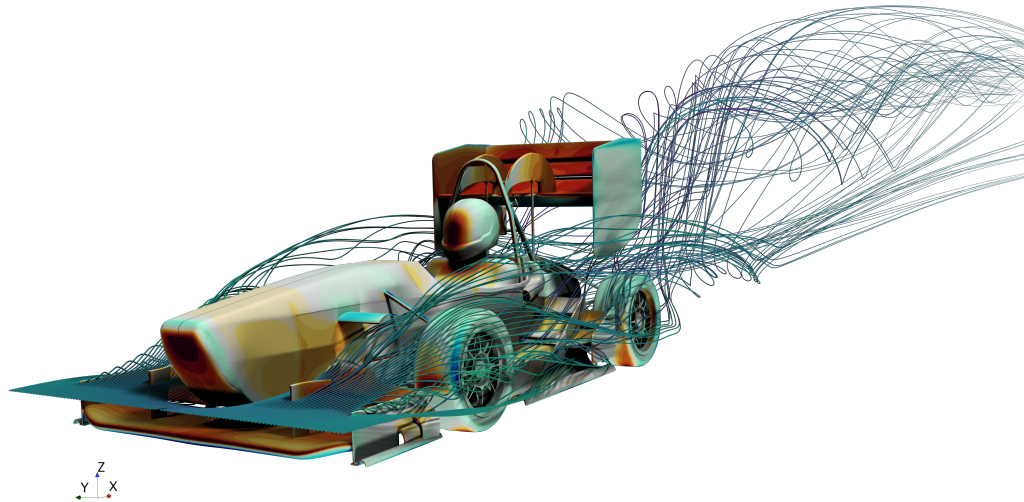


Figure 1.2: Total Pressure Coefficient + Streamlines SC23

Squadra Corse is the Formula Student team of the Politecnico di Torino. For the 2021/22 and 2022/23 seasons, I was head of the Aerodynamics and CFD division. The division is responsible for designing the car's aerodynamic package through the use of CAD and CFD simulations. In addition to the design work, the division

also has the task of laminating the various components and assembling the package. The aerodynamic package is mainly divided into four macro areas:

- Front Wing
- Rear Wing
- Sidepods
- Undertray

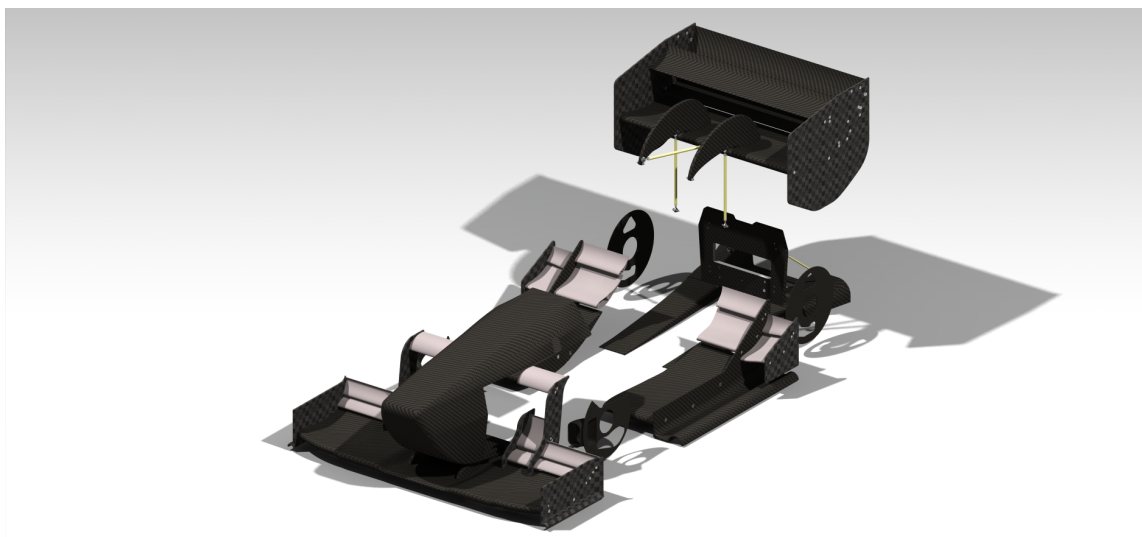


Figure 1.3: Aeropack SC22

As Head of the Aerodynamics and CFD division my tasks are:

- Lead the aero development and performance of the vehicle
- Coordinate the car performance with other departments
- Responsibility for the development of the correlation metrics, tools and methodology
- Set up aerodynamic performance targets.

1.3 Background and Motivation

Aerodynamics plays a pivotal role in the modern race car. Accurate prediction of aerodynamic performance is crucial for designing an efficient aeropack. Computational Fluid Dynamics (CFD) has emerged as a valuable tool for simulating the

complex flow interactions that occur around the vehicle. However, ensuring the accuracy of CFD simulations and their ability to predict real-world aerodynamic behavior is essential.

The motivation behind this thesis lies in enhancing the accuracy of CFD simulations for race car aerodynamics, ultimately leading to improved vehicle performance and a competitive advantage on the track.

- **Performance Gains:** In motorsports, even the slightest improvement in aerodynamic efficiency can translate to significant performance gains. Validating CFD simulations against real-world data allows engineers to fine-tune aerodynamic features to optimize downforce, minimize drag, and achieve better lap times.
- **Design Iteration:** Motorsports teams are constantly refining their race car designs. Validated CFD models enable rapid design iteration by providing insights into how modifications to aerodynamic components, such as wings, diffusers, and splitters, impact overall performance.
- **Cost and Time Savings:** Physical wind tunnel testing and track testing are resource-intensive processes. Validated CFD simulations can replace some of these tests, leading to cost and time savings during the design and development phase.
- **Safety and Stability:** Accurate CFD simulations help engineers understand how aerodynamic forces influence the car's stability and handling characteristics. This insight is crucial for designing cars that maintain stability at high speeds and through various driving conditions.
- **Advancing Motorsport Engineering:** Successfully validating CFD models for race car aerodynamics contributes to the broader field of vehicle aerodynamics and fluid dynamics research. It provides valuable data for improving simulation techniques and understanding complex flow phenomena.

1.4 Research Objectives

The main goal of this thesis is to validate the accuracy of the CFD model developed. This involves comparing the results of the CFD simulations with real-world wind tunnel test data. By doing so, it is ensured that the model is capable of predicting the aerodynamic behavior of the car accurately. This step is crucial because it establishes the credibility and reliability of your CFD simulations.

Once the model is validated, it can be possible to use it to identify areas of the car's aerodynamics that can be improved. This might involve making design changes to

reduce drag, increase downforce, or optimize airflow around the car. The aim is to exploit the validated CFD model to enhance the car's overall performance, which could lead to better speed, stability, and fuel efficiency.

With a validated CFD model available, you can delve into a deeper analysis of the car's behavior under various dynamic conditions. This includes not only understanding how the car behaves under standard driving conditions but also exploring more complex scenarios, such as cornering. By simulating these scenarios, you can gain insights into how the car's aerodynamics impact its handling, stability, and overall performance.

A specific aspect of the car's behavior of really importance is its aerodynamics during cornering. Developing aerodynamic maps involves creating a comprehensive understanding of how the car's aerodynamic forces change as it goes through different degrees of cornering. This can be particularly useful for racing applications or any situation where the car's lateral dynamics are critical. By creating these maps, you can optimize the car's design and setup for enhanced cornering performance.

Chapter 2

Literature Review

This chapter is meant to give some brief relevant background information in CFD modelling. The reader is assumed to have some background knowledge in aerodynamics.

2.1 Overview of CFD Modeling

Computational Fluid Dynamics (CFD) modeling is a branch of fluid mechanics that deals with the numerical simulation of fluid flows and heat transfer phenomena. It's widely used in engineering and scientific research to analyze and predict the behavior of fluids and gases in various scenarios. CFD modeling involves the application of mathematical equations that govern fluid flow and heat transfer to a discrete grid, allowing for the simulation of complex fluid interactions that might be difficult or impossible to solve analytically.

Any fluid flow are governed by three fundamental principles: mass is conserved; Newton's second law ($F = ma$); and energy is conserved. These fundamental physical principles can be expressed in terms of basic mathematical equations, which in their most general form are either integral equations or partial differential equations. Computational fluid dynamics is the art of replacing the integrals or the partial derivatives (as the case may be) in these equations with discretized algebraic forms, which in turn are solved to obtain numbers for the flow field values at discrete points in time and/or space.[2]

2.1.1 Governing Equation

CFD is based on fundamental equations of fluid mechanics, namely the Navier-Stokes equations for fluid motion and the heat conduction equation for heat transfer.

These equations describe the conservation of mass, momentum, and energy in a fluid.

This approach is possible only if we consider valid the following hypotheses:

- Continuous flow;
- Non-reacting and homogeneous flow;
- Flow without electrical charges.

Continuous flow hypothesis deals with the mean free path, a concept used in physics to describe the average distance a particle or photon can travel through a medium before encountering a collision with another particle. The mean free path, often denoted by the symbol λ (lambda), is calculated as:

$$\lambda = \frac{1}{\sqrt{2}n\sigma} \quad (2.1)$$

where:

- n is the number density of particles in the medium
- σ is the collision cross-section, which represents the effective area that a particle presents for collisions

The Knudsen number (K_n) is a dimensionless parameter used in the field of gas dynamics to characterize the relative importance of molecular mean free path to a characteristic length scale of a flow system. It is particularly relevant in situations where the mean free path of gas molecules becomes comparable to or larger than the physical dimensions of the system. It is defined as:

$$K_n = \frac{\lambda}{L} \quad (2.2)$$

where L is a characteristic length scale of the system, such as the radius of a pipe, the width of a channel, or the size of a solid object.

The Knudsen number helps determine whether a gas flow can be accurately described using continuum assumptions (i.e., treating the gas as a continuous fluid) or whether rarefied gas dynamics must be considered due to significant molecular interactions. The interpretation of the Knudsen number is as follows:

- $Kn \ll 1$: In this regime, the molecular mean free path is much smaller than the characteristic length scale. The gas behaves as a continuum, and macroscopic fluid dynamics equations (e.g., Navier-Stokes equations) are applicable;

- $\text{Kn} \approx 1$: When the Knudsen number is of the order of unity, the gas flow is in the transition regime between continuum and rarefied flow. Both molecular and continuum effects play a role, and specialized models like the slip-flow model may be required.
- $\text{Kn} \gg 1$: In this regime, the molecular mean free path is much larger than the characteristic length scale. The gas is in a rarefied state, and molecular interactions dominate over continuum behavior. Rarefied gas dynamics equations, such as the Boltzmann equation, become necessary for accurate modeling.

Continuity Equation

The continuity equation is a statement of mass conservation. It states that the rate of change of mass within a control volume is equal to the net rate of mass flow into the control volume. Mathematically, the continuity equation can be written as:

$$\frac{\partial \rho}{\partial t} + \nabla(\rho \vec{u}) = 0 \quad (2.3)$$

where:

- ρ is the density of the fluid;
- \vec{u} is the velocity vector ($u\mathbf{i} + v\mathbf{j} + w\mathbf{k}$).

Momentum Equation

The momentum equation states that the net change of momentum in any direction is due to the sum of the pressure, dissipative and body forces exerted. Mathematically, the momentum equation can be written as:

$$\frac{\partial(\rho \vec{u})}{\partial t} + \nabla(\rho \vec{u} \vec{u}) = -\nabla p + \nabla \cdot \bar{\bar{\tau}} + \rho \vec{f} \quad (2.4)$$

where:

- ρ , Density of the fluid;
- \vec{u} , Velocity vector ($u\mathbf{i} + v\mathbf{j} + w\mathbf{k}$);
- τ , Stress Tensor;
- p , Pressure;
- f , Body Forces.

Energy Equation

The third equation takes into account the rate of change of the total energy owing to the net heat flux towards the control volume plus work done per time unit on the control volume by volumetric and surface forces. Mathematically, the energy equation can be written as:

$$\frac{\partial E}{\partial t} + \nabla \cdot (E\vec{u}) = \rho\dot{\zeta} - \nabla \cdot \dot{\vec{q}} - \nabla \cdot (p\vec{u}) + \nabla \cdot (\bar{\tau}\vec{u}) + \rho\vec{f} \cdot \vec{u} \quad (2.5)$$

where:

- $\dot{\zeta}$, Heat Absorbed per unit time and unit mass;
- $\dot{\vec{q}}$, Heat Flux due to thermal conduction where k is the conduction constant;
- $E = e + \frac{|\vec{u}|^2}{2}$, Total Energy per unit volume as sum of internal energy e and kinetic energy;
- $p\vec{u}, \bar{\tau}\vec{u}, \rho\vec{f} \cdot \vec{u}$, Work done by Pressure, Viscosity Dissipation and Body Forces.

Closure problem

As it is possible to note, the Navier-Stokes laws are 5 equations in 14 unknowns that are:

- ρ , Density;
- u_i , three components of velocity;
- T , Temperature;
- p , Pressure;
- e , Internal Energy;
- τ_{ij} , six components of Stress Tensor;
- μ , Viscosity.

For this reason it is necessary to add other equations to close the problem. The temperature can be expressed through the Ideal Gas law:

$$T = \frac{p}{\rho R^*} \quad (2.6)$$

with $R^* = \frac{R}{M}$ where R is the universal gas constant and M is the molar mass. The Stress Tensor, indeed, derives by the viscosity Newton's law:

$$\tau_{ij} = \mu \left(\frac{\partial u_i}{\partial x_j} + \frac{\partial u_j}{\partial x_i} \right) \quad (2.7)$$

where μ is the dynamic viscosity of the fluid which, in turn, depends on pressure and temperature: $\mu = \mu(p, T)$. At the end, the Internal Energy is a function of Temperature and it is stated as: $e = c_v T$, where c_v is the Specific Heat considering constant volume. Now, the problem is a closed system but, unfortunately, there is not any analytical solution; only in some rare and really simple cases.

2.1.2 Discretization Methods

Discretization is a fundamental step in Computational Fluid Dynamics (CFD) where continuous governing equations that describe fluid flow are approximated using discrete methods in order to solve them on a numerical grid. There are several discretization methods commonly used in CFD, with Finite Difference, Finite Volume, and Finite Element being the most prominent ones. Here a brief overview of each:

- **Finite Difference Method (FDM):** This method involves approximating derivatives in the governing equations using finite difference approximations. The domain is discretized into a grid, and the equations are evaluated at discrete points on the grid. Central differences, backward differences, and forward differences are commonly used to approximate derivatives. FDM is relatively simple and intuitive, making it a good starting point for understanding numerical methods.
- **Finite Volume Method (FVM):** The finite volume method focuses on conservation principles. The domain is divided into control volumes, and the integral form of the governing equations (such as the conservation of mass, momentum, and energy) is applied to each control volume. This method is well-suited for dealing with complex geometries and unstructured grids. It maintains conservation properties well and is widely used in commercial CFD software.
- **Finite Element Method (FEM):** While originally developed for structural analysis, the Finite Element Method has been extended to fluid dynamics. FEM involves discretizing the domain into smaller elements, and within each element, the equations are approximated using basis functions. These basis functions allow for more flexibility in handling irregular geometries and can provide accurate results with adaptive mesh refinement. FEM is also used for solving problems involving fluid-structure interaction.

Mesh Grid

In the context of computational fluid dynamics (CFD), a mesh refers to the discretization of the computational domain into a collection of smaller geometric elements, such as triangles or quadrilaterals in two dimensions, and tetrahedra or hexahedra in three dimensions. This meshing process is essential because it transforms the continuous equations governing fluid flow into a set of discrete equations that can be solved numerically on a computer.

Mesh types can be classified into the following categories:

- **Structured Mesh:** In a structured mesh, the grid elements (cells) have a regular geometric shape, such as rectangles in 2D or hexahedra in 3D. The cells are aligned with each other and the domain boundaries. Structured meshes are relatively easy to generate and can be efficient for simple geometries, but they might struggle to represent complex shapes accurately;
- **Unstructured Mesh:** Unstructured meshes consist of grid cells with irregular shapes, such as triangles in 2D or tetrahedra in 3D. Unstructured meshes are more flexible and can accurately represent complex geometries. They are often preferred for simulations involving intricate flow patterns and irregular shapes;
- **Hybrid Mesh:** A hybrid mesh combines both structured and unstructured elements. This approach is useful when different parts of the domain have varying levels of complexity. For example, structured elements might be used in simpler regions, while unstructured elements are employed in more complex areas.

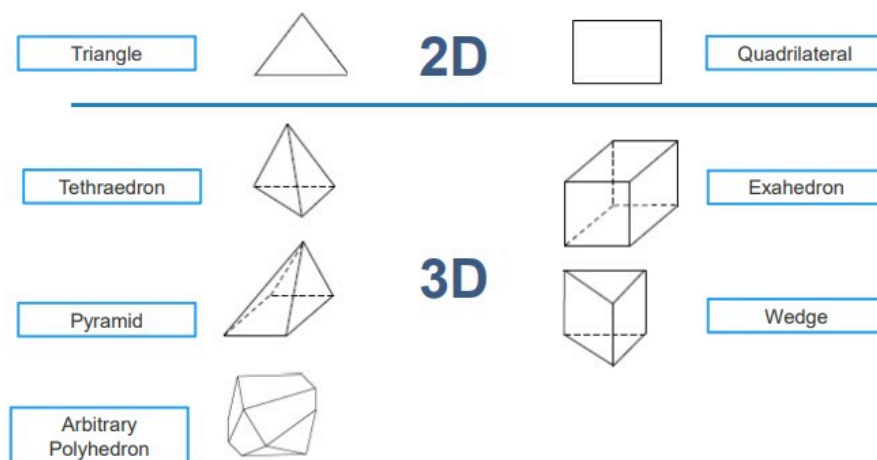


Figure 2.1: Classification of Cell Type [3]

The accuracy and efficiency of a CFD simulation heavily depend on the quality of the mesh. We measure the mesh quality, using a set of quality metrics. The quality metrics determine how far we are from an ideal cell shape. Here some important quality parameter:

- **Aspect Ratio:** Aspect ratio is the ratio of a cell's longest length to the shortest length. The ideal aspect ratio is 1. The smaller it is, the higher the quality of an element is;
- **Non-orthogonality:** Non-orthogonality is the angle between the vector connecting two adjacent cell centers and the normal of the face shared by these cells. The range of non-orthogonality is between 0 (ideal) and 90 (worst). 0 indicates the mesh being orthogonal. Two perfect hexes aligned with each other have non-orthogonality equal to 0. Non-orthogonal grids can introduce artificial diffusion effects in the simulation, which can alter the behavior of the flow and reduce the ability to capture fine-scale flow features accurately. It is recommended to keep the non-orthogonality below 70;
- **Skewness:** Skewness is usually quantified using an angle or a numerical value that indicates how far a cell's shape deviates from an ideal shape. The angle between the cell's diagonals or the ratio of the shortest edge to the longest edge are common measures of skewness. The skewness value is often normalized to a range of 0 to 1, where 0 represents an ideal, perfectly orthogonal cell, and 1 represents a highly skewed or distorted cell. The calculation method varies by the cell type as follows:

➤ **Hexahedral cell:**

$$Skewness = \max \left[\frac{\theta_{MAX} - 90^\circ}{90^\circ}, \frac{90^\circ - \theta_{MIN}}{90^\circ} \right] \quad (2.8)$$

➤ **Tetrahedral cell:**

$$Skewness = \frac{cellsize(Optimal) - cellsize}{cellsize(Optimal)} \quad (2.9)$$

2.1.3 Turbulence Models

Turbulence models are mathematical approaches used in CFD to simulate and predict the behavior of turbulent flows. Turbulence, characterized by chaotic and irregular fluid motion, is a complex phenomenon that spans a wide range of scales, making it challenging to model accurately. Turbulence models introduce simplifications and assumptions to describe the effects of turbulence on the mean flow properties without resolving all the intricate details of the turbulent fluctuations.

Here is a list of some commonly used turbulence models in computational fluid dynamics:

- **Reynolds-Averaged Navier-Stokes (RANS) Models**

- **k-epsilon Model:** This is one of the most widely used RANS models. It solves for two additional transport equations: one for turbulent kinetic energy (k) and another for its dissipation rate (ϵ). It's suitable for a wide range of flows and offers a good balance between accuracy and computational cost;
- **k-omega Model:** Similar to the k-epsilon model, this model also solves for turbulent kinetic energy (k) and its dissipation rate (ω). It is known for better performance in adverse pressure gradient flows and near-wall regions;
- **Spalart-Allmaras Model:** This one-equation model is designed to capture boundary layer behavior and is often used in aerospace applications. It solves for the eddy viscosity and includes a transport equation for the turbulence-specific variable, which models the turbulence production, dissipation, and convection;
- **Reynolds Stress Model (RSM):** Unlike some other turbulence models that focus on modeling the turbulent kinetic energy and its dissipation rate, RSM directly solves for the individual components of the Reynolds stress tensor. The Reynolds stress tensor captures the correlations between velocity fluctuations in different directions and provides more detailed information about the anisotropic nature of turbulence.

- **Large Eddy Simulation (LES):** LES is an approach that directly resolves the large-scale turbulent structures while modeling the smaller scales. It's suitable for flows where large eddies dominate. LES provides more accurate results compared to RANS models but requires more computational resources;
- **Direct Numerical Simulation (DNS):** DNS directly solves the Navier-Stokes equations without any turbulence modeling. It provides the most accurate results but is computationally expensive and limited to relatively low Reynolds number flows.

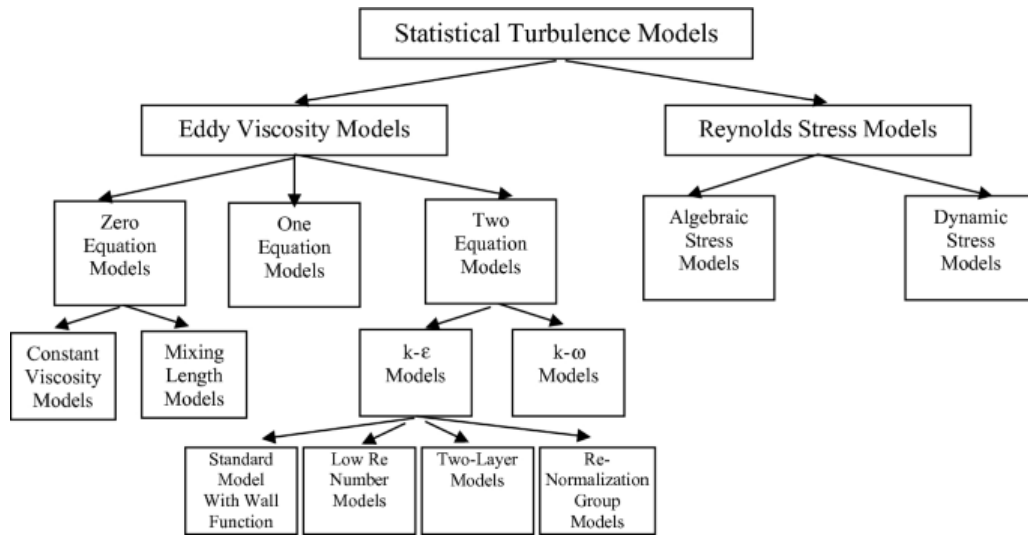


Figure 2.2: Turbulence Model - RANS [4]

Reynolds-Averaged Navier-Stokes (RANS) Models

In real phenomena, most flows are turbulent and they can be characterized by several properties:

- Highly unsteady condition with substantial cycle-to-cycle fluctuations;
- Turbulent mixing, generating a phenomenon known as turbulent diffusion. This process brings about dissipation, where the transformation of kinetic energy into internal energy takes place;
- Vortex stretching, which increases turbulence;
- Both large-scale and small-scale turbulent motions are present. [5]

A normal engineering approach is to use the Reynolds-Averaged-Navier-Stokes equations which are applied when the flow is statistically steady. In steady turbulent flow fields, every variables can be written as the sum of a time-averaged value and a fluctuation:

$$\phi(x_i, t) = \overline{\phi(x_i)} + \phi'(x_i) \quad (2.10)$$

where \overline{U} is the average velocity and $u(t)$ is the turbulent fluctuation component. Mean velocity:

$$\overline{\phi(x_i, t)} = \lim_{T \rightarrow \infty} \frac{1}{T} \int_{t_0}^{t_0+T} \phi(x_i, t) dt \quad (2.11)$$

with t equals to time and T to averaging interval, which has to be greater than the usual timeframe of the variations.

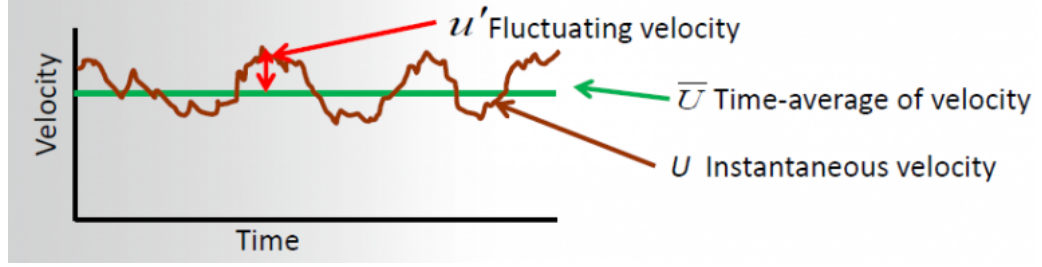


Figure 2.3: Instantaneous Velocity

By doing so, the variable becomes independent of the specific moment at which the averaging process commences.

In this way the averaging fluctuations are null while from the quadratic quantities two new terms are obtained:

$$\overline{u_i \phi} = \overline{(\bar{u}_i + u'_i)(\bar{\phi} + \phi')} = \bar{u}_i \bar{\phi} + \overline{u'_i \phi'} \quad (2.12)$$

Introducing the 2.12 in the conservations equations for an incompressible flow, we obtain:

$$\nabla \cdot \vec{V} = 0 \quad (2.13)$$

$$\frac{\partial \bar{u}_i}{\partial t} + \frac{\partial}{\partial x_j} (\bar{u}_i \bar{u}_j) + \frac{\partial}{\partial x_j} (\overline{u'_i u'_j}) = -\frac{\partial \bar{p}}{\partial x_i} + \mu \frac{\partial}{\partial x_j} \left(\frac{\partial \bar{u}_i}{\partial x_j} + \frac{\partial \bar{u}_j}{\partial x_i} \right) - \frac{\partial}{\partial x_j} (\overline{\rho u'_i u'_j}) \quad (2.14)$$

The additional term $-\overline{\rho u'_i u'_j}$ in the averaged momentum equations is called as **Reynolds Stress Tensor**. This is due to fluctuating velocities in turbulent flows, which enhance the momentum of fluid flows. s. It means that the problem is not closed and, consequently, some approximations are needed to prescribe them in terms of the mean quantities. The additional term in RANS equations is calculated based on turbulent models.[6]

Chapter 3

Methodology

This chapter deals with the preparation of the geometry, the setting up of the mesh of the computational fluid domain and the performance analysis. The SC22 is a Formula Student car entirely designed by the Squadra Corse PoliTo team. This vehicle has participated in the Varano (Formula ATA), Hockenheim (FSG) and FS Alpe Adria events, achieving a second place in the Engineering Design Event, a third place in the Cost Event and two second places in the Skidpad and Autocross Event.



Figure 3.1: SC22 - Varano

3.1 Geometry and Mesh Generation

The geometry developed for this thesis was designed with CATIA V5 by members of the Squadra Corse team.

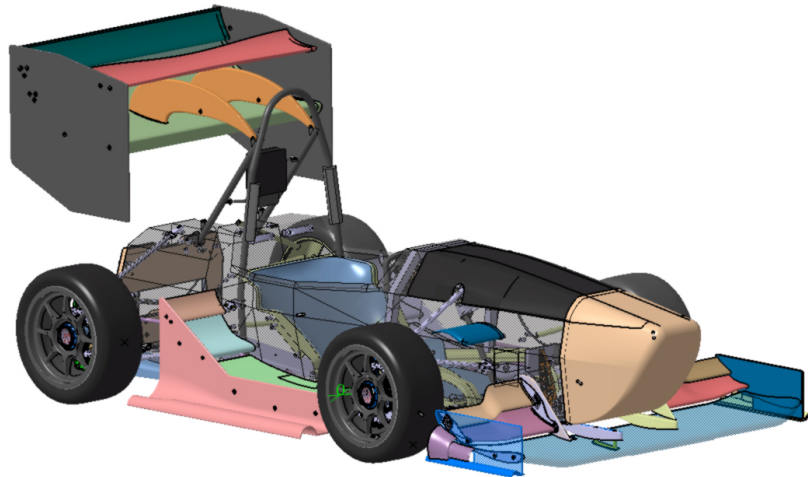


Figure 3.2: SC23 - CATIA

From the CATIA model, the surfaces of interest were extracted and passed to the commercial software **BETA CAE ANSA**. Through this software, geometry clean-up was carried out due to its ease in handling complex geometries. The advantages are:

- Creation of the water-tight domain directly, avoiding problems correlated to the *Subtract* function in STAR-CCM+
- Possibility to simplify the geometry when needed (e.g. suspensions assembly)
- Definition of each part (different colors in the image), for further in-depth analysis (forces on a component mainly useful for FEMs)

The calculation domain was set in order to reach a Blockage Ratio $<1\%$. The computational domain has the following dimensions:

$$15L \times X7W \times X10H$$

where:

- L = Length of the car
- H = Height of the car
- W = Half Width of the car (symmetric domain)

The x-dimension is repered in $5L$ ahead of the car and $9L$ behind the car.

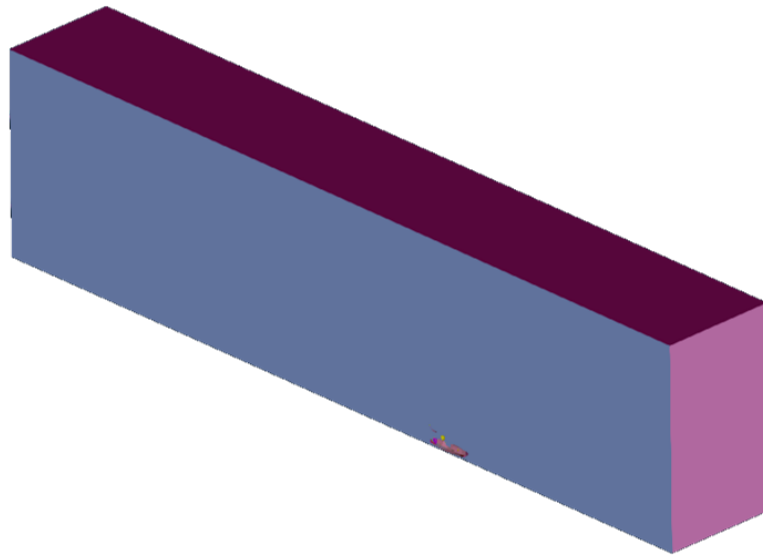


Figure 3.3: Domain - BETA CAE ANSA

Now that the geometry has been prepared, the computational fluid domain can be created using the best practice sizes by the Simcenter *Guidelines for FSAE cars* [7]. For the aim of the longitudinal aerodynamic analysis, the simulation will be processed only using half a car.

Main characteristics:

- Trimmed mesh (highly recommended and more developed on STAR-CCM+, also requires less RAM)
- Prism Layers for wall resolution
- Base size (BS) = 48 mm
- Refinement boxes in % of the base size, for Grid Convergence study
- Polyhedral mesh in the MRF zone

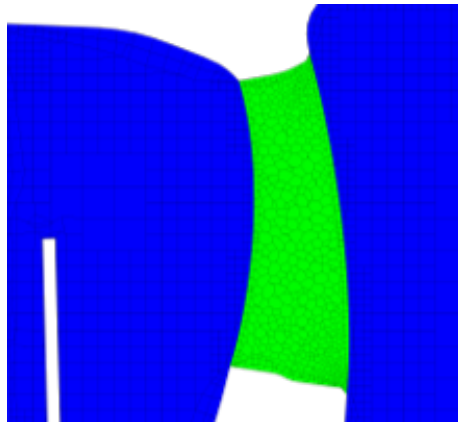


Figure 3.4: Detail of MRF zone (green) with polyhedral mesh

BOX REFINEMENTS	Percentage of BS
Wings, Wheels	12,5%
Surface Offset	50%
Leading and Trailing edges	6,125%
Wake	75%
Far Field	300%

Table 3.1: Mesh refinement

Simcenter STAR-CCM+

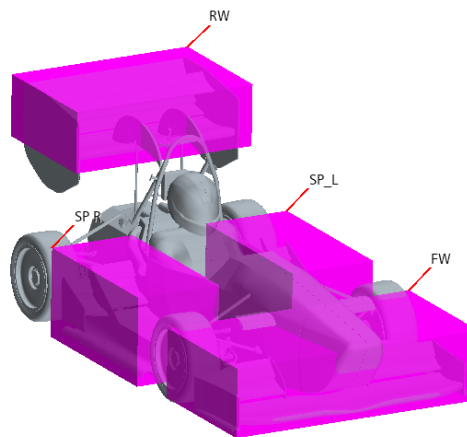


Figure 3.5: Example of Box Refinements (Wings)

Regarding the refinement in the wake, the process began with a standard box. After conducting the initial simulations, two isosurfaces of the total pressure coefficient were extracted from them at values of approximately 0.5 and 0.9, respectively, to cover the entire wake region of the machine. The isosurface with the smaller value was used for finer refinement, while the one with the larger value was used for "coarser" refinement.

The last step of the setting up of the mesh deals with the improvement of the mesh and the meshing process of the prism layer for the boundary layer capture. The boundary layer, with its asymptotic behavior, is amenable to analysis through the use of dimensionless variables. This characteristic is often referred to as "Wall Similarity", which is crucial for establishing a framework to distinctly define the scales of viscosity fluctuations within this region. In essence, Wall Similarity enables us to uniquely characterize the behavior of these fluctuations in relation to the boundary layer. To find them, friction velocity u_τ and scale length l_ν are introduced:

$$u_\tau = \sqrt{\frac{\tau_w}{\rho}} \quad l_\nu = \frac{\nu}{u_\tau} \quad (3.1)$$

where τ_w is the wall stress computed by Newton's law and, through these variable, is possible to evaluate the non-dimensional velocity and length, called inner variables:

$$u^+ = \frac{u}{u_\tau} \quad y^+ = \frac{y}{l_\nu} = \frac{u_\tau y}{\nu} \quad (3.2)$$

Calculating the laminar boundary layer is relatively straightforward because it comprises a single layer. In contrast, dealing with the turbulent boundary layer is considerably more complex. This complexity arises from the fact that the boundary layer can be divided into two distinct regions: an outer layer, connecting it to the undisturbed flow, and an inner layer, which is a multi-layered zone.

1. **Viscous Sublayer:** $0 \leq y^+ \leq 5$ $u^+ = y^+$
in this region the viscous forces are predominant over the inertial ones (low Re);
2. **Viscous Sublayer:** $5 < y^+ < 30$
it is a mixing zone where there is the maximum production of turbulent kinetic energy and the viscous and inertial forces are comparable;
3. **Logarithmic Layer:** $y^+ > 30$ $u^+ = \frac{1}{k} \ln(y^+) + C$
where $k = 0.41$ is the Von Karman constant and $C = 5$ is the Coles constant; the inertial forces become predominant over the viscous ones (high Re).

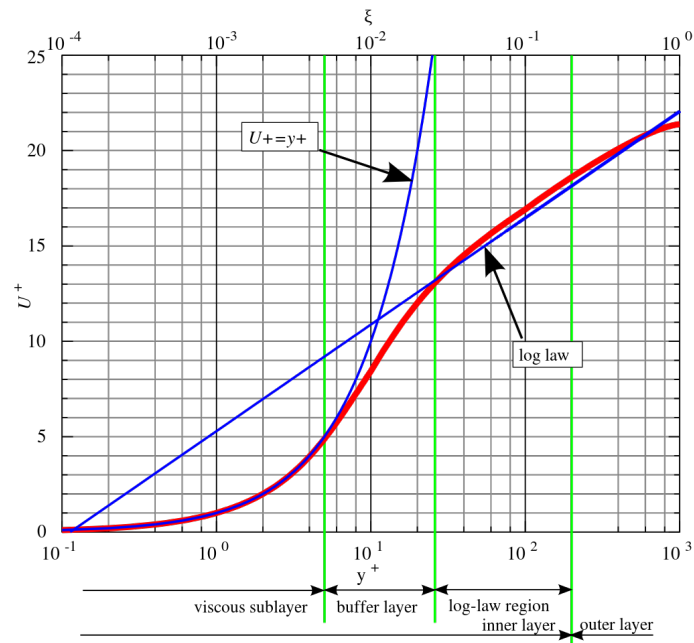


Figure 3.6: Inner Layer

The wall treatment approach used is the **all y^+ wall treatment model**. This means:

- **Low y^+** approach on wings and body-work where maximum accuracy on separation is needed
- **High y^+** approach on surfaces where intense separation is expected and less precision is needed

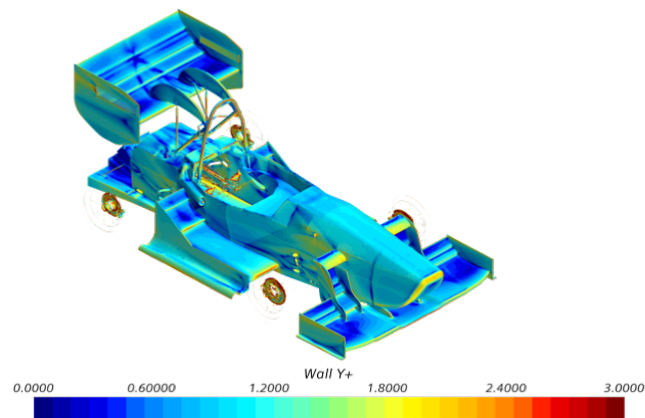


Figure 3.7: Low y^+

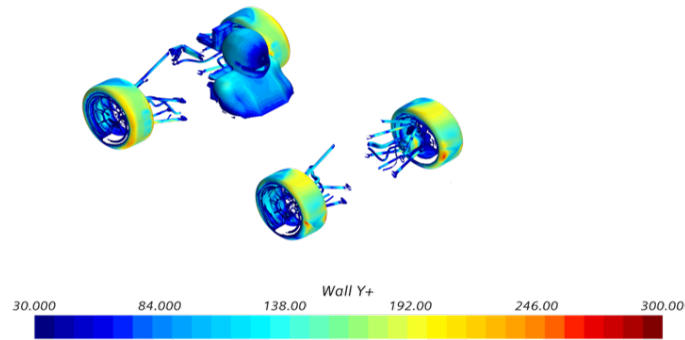


Figure 3.8: High y^+

Prism Layers are defined on each component, based on the y^+ target value.

- total height (firstly estimated through turbulent flat plate formula)
- near-wall-thickness (estimated through the y^+ target)
- number of layers (12 layers for wings , 8 for body-work)

Along with y^+ , turbulent viscosity ratio is utilized to check if the boundary layer is well modelled.

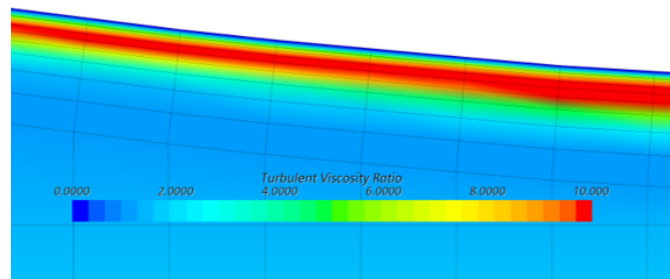


Figure 3.9: Turbulent Viscosity Ratio

3.2 Boundary and Initial Conditions

In the computational fluid dynamics (CFD) simulation being described, various boundary conditions have been applied to capture the behavior of a system involving fluid flow, potentially related to a vehicle or similar scenario. These boundary conditions are essential for setting up the simulation and ensuring accurate results.

Here's an explanation of each of the specified boundary conditions:

- **Velocity Inlet:** A velocity inlet condition is applied with an incoming velocity of $[60, 0, 0]$ kph. This means that fluid is entering the simulation domain at a speed of 60 kilometers per hour in the x-direction (horizontal);
- **Pressure Outlet:** The outlet boundary condition is set as a pressure outlet with a pressure of 0 Pascals (Pa). This represents an assumption that the fluid exits the system with zero pressure;
- **Symmetry Plane:** Symmetry planes are placed on the centerline of the simulation domain. These symmetry planes are used to simplify the simulation by assuming that fluid behavior on one side of the plane is mirrored on the other side. This condition is typically used to reduce computational complexity in cases where the system exhibits symmetry;
- **Ground Velocity:** The ground is assigned a velocity of $[60, 0, 0]$ kph. This indicates that the ground is moving at the same speed as the velocity inlet condition, suggesting a scenario where the ground is part of the moving reference frame;
- **Local Rotation Rate for Wheels and Brake Discs:** This condition likely represents the rotation of vehicle wheels and brake discs. It implies that these components are allowed to rotate locally at a certain rate, which is not specified in the provided information;
- **Contact Patches with Imposed Velocity:** Contact patches are regions within the simulation where a specific velocity of $[60, 0, 0]$ kph is imposed. This could represent surfaces or components of the vehicle that are in contact with the fluid, and their motion is prescribed;
- **MRF Regions with Local Rotation Rate for Air Between Rims:** Multiple Reference Frame (MRF) regions are defined in the simulation. These regions are typically used to model rotating components like the rims of a vehicle. In this case, local rotation rates for the air between the rims are specified. This condition helps account for the interaction between rotating parts and the surrounding air.

These boundary conditions collectively define the behavior of the fluid and its interaction with the components and surfaces in the simulation domain. They are crucial for obtaining meaningful results from CFD simulations, especially in scenarios involving complex fluid-solid interactions, such as vehicle aerodynamics or fluid dynamics around rotating components.

For what concern the radiator modelling a porous medium approach has been adopted. In Computational Fluid Dynamics (CFD), a porous zone or porous medium is a modeling approach used to simulate the behavior of fluid flow through a region that contains a porous material, such as a porous solid, foam, or a filter. Porous zones are commonly used in CFD simulations to represent situations where fluid flow through a solid material is of interest, such as in heat exchangers, catalytic converters, or filters.

The resistance is calculated with respect to the local axis of the radiator, which presents an angle with the simulation coordinate system.

$$F = -P \cdot v \quad (3.3)$$

$$P = P_v + P_i \cdot |\nu| \quad (3.4)$$

$$\Delta p = F/A \quad (3.5)$$

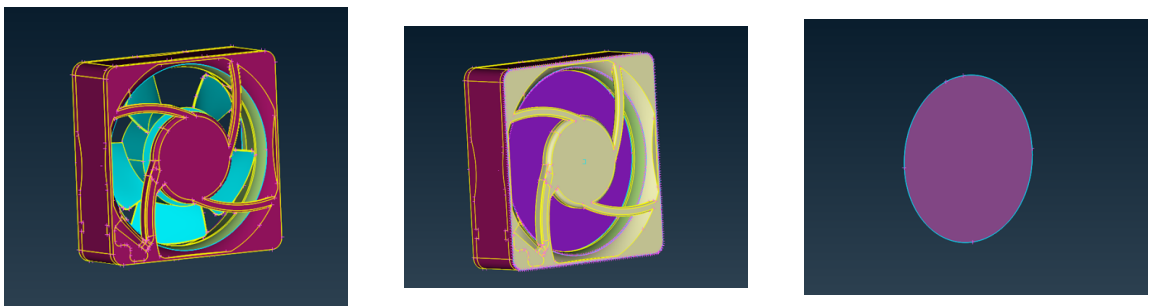
Porous Inertial P_i	$150kg/m^4$
Porous Viscous P_v	$500kg/(m^3s)$

Table 3.2: Porous Media

This values are referred to the z-axis of the radiator.

Starting from the CAD reproduction of the 4100 N-2H8P fan, three configurations were tested in a 0-loss domain:

1. MRF of the whole Fan Region;
2. Fan Interface inside the case;
3. Fan Interface substituting the whole fan;



(1)

(2)

(3)

Figure 3.10: Fans Modelling

Configuration	Δp [Pa]	\dot{m} [kg/s]	\dot{V} [m^3/s]	Efficiency (*)
MRF Fan	410	0,165	501,63	/
Fan Interface in the case	371	0,159	484,08	0,8
Fan interface alone	260	0,172	522,91	0,8

Table 3.3: Fans Modelling Results

(*) η is assigned to the Fan Interface as an input for the «swirl» option and can be calculated as follows:

$$\eta = \frac{Power\ Imparted\ to\ Air}{Power\ Consumed} = \frac{\dot{V} \Delta P_t}{\dot{m} \Omega r \Delta V_t} \quad (3.6)$$

where:

- \dot{V} : Volumetric Mass Flow Rate [m^3/s]
- ΔP_t : Difference of Total Pressure between Inlet and Outlet [Pa]
- \dot{m} : Mass Flow Rate [kg/s]
- Ω : Angular Speed [rad/s]
- r : Radius of the Fan [m]
- ΔV_t : Difference of speed between Inlet and Outlet of the Fan [m/s]

Results have been compared with datasheet. Best configuration was identified in the Fan Interface alone, since it led to values similar to datasheet in the working point and also is less computational demanding.

Efficiency η was tested and the best configuration (in terms of datasheet fit) resulted in the «no swirl» one. Datasheet curve is reproduced through an Excel sheet and put on STAR-CCM+ in terms of polynomial piecewise functions.

The same approach is applied both for radiators fan and battery pack fans.

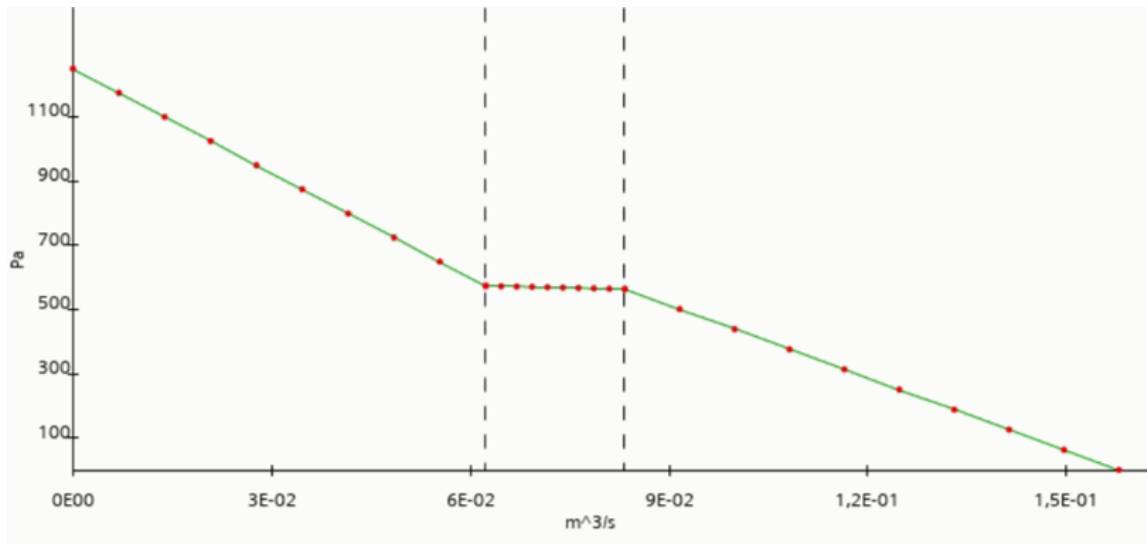


Figure 3.11: Fan Curve STAR-CCM+

3.3 Numerical Methods

In the realm of computational fluid dynamics (CFD), the successful simulation of fluid flow and its associated phenomena hinges on the selection of appropriate physics models and solvers. In this specific case, the following physics models and solver configurations have been employed:

- **RANS Equations (Reynolds-Averaged Navier-Stokes):** RANS equations provide a practical framework for modeling turbulent flows. They involve the Reynolds decomposition of flow variables into mean and fluctuating components, enabling the simulation of time-averaged flow characteristics.
- **Steady State Solver:** Utilizing a steady-state solver implies that the simulation assumes that the flow variables do not change with time. This simplification is often justified for cases where the flow has reached a stable, time-independent state.
- **Incompressible Flow:** The assumption of incompressibility is valid when the flow's Mach number (M) is sufficiently low (in your case, $M=0.048$). This means that density variations due to flow velocity are negligible, simplifying the equations and making it appropriate for modeling at low speeds.
- **Turbulence Model - $k-\omega$ SST (Shear-Stress Transport):** The $k-\omega$ SST turbulence model is a widely used closure model for turbulent flows. The SST $k-\omega$ model is a two-equation model that solves for two variables:

the turbulence kinetic energy (k) and the specific dissipation rate (ω). It effectively combines the k - ω model in the near-wall region, which is particularly suitable for capturing wall-bounded turbulent flows, with the k - ϵ model in the free-stream region, where turbulence is less influenced by the wall.

- **Segregated Flow:** The segregated flow solver typically separates the calculation of different flow variables, such as pressure and velocity, into distinct computational steps. This approach can be more computationally efficient and is often used in CFD simulations.
- **All $y+$ Wall-Treatment:** Employing the *all $y+$ wall-treatment* indicates that the turbulence model and solver are designed to handle a wide range of near-wall conditions (represented by $y+$, which is the dimensionless wall distance) effectively. This ensures accurate modeling of the boundary layer and near-wall turbulence.

Chapter 4

Validation Case

In the pursuit of scientific knowledge and the advancement of our understanding in various fields, it is imperative that research findings are not merely accepted at face value but are subjected to rigorous examination. This chapter, the Validation Case, marks a pivotal phase, where I am going to scrutinize, evaluate, and validate the findings, hypotheses, and models presented in the preceding chapters. The central purpose of this chapter is to provide evidence supporting the reliability and validity of the CFD model.

The significance of validating the CFD simulations cannot be overstated. While CFD offers the promise of cost-effective and detailed analyses of complex fluid behaviors, its utility hinges upon the accuracy and reliability of the computational models employed.

The aims of this chapter are: reaffirm the credibility of the CFD simulations and contribute to the broader body of knowledge in the field of fluid dynamics.

Within the following sections, I am going to deeply analyse the methodologies and strategies employed to validate the CFD models. I will then outline the extensive efforts undertaken to ensure that numerical predictions align with experimental data and established physical principles.

Throughout this chapter, I am aware of the need to address limitations and uncertainties in this work: every model, no matter how sophisticated, is an approximation of reality. By presenting these limitations, the aim is to facilitate a better understanding of the applicability and boundaries of CFD simulations.

What will be now discussed and presented are the examination and validation of the computational model characterising the core of the research presented in this thesis.

4.1 Experimental Data

For validation of the CFD model, the car was taken to the FCA wind tunnel in Orbassano.

The FCA wind tunnel facility in Orbassano (Italy) is a closed-circuit type (Gottinga) with 3/4 open jet test section (10.5 m long, 12 m wide and 12 m tall), a 30.5 m^2 nozzle cross section (contraction ratio 4:1) and a maximum inflow velocity of 200 kph.

The rolling road simulation system (RRSS) provides a 5-belts configuration: one central narrow belt, 6-meter length, 1.1 meter width, and four wheel spinning units. The main balance is integrated within the RRSS. The main balance is integrated within the RRSS. Possibly, the whole platform can rotate around the vertical axis for yaw tests.

The combination of boundary layer suction system effect and moving belt produces a nearly zero height displacement thickness ($\delta^* < 0.5 \text{ mm}$) along the entire main belt. Furthermore, four additional balances under the wheel spinning units measure tangential forces necessary to keep constant rotational wheel speed and, in this way, to measure the sum of drag forces (mechanics, tyre rolling resistance and wheel ventilation).



Figure 4.1: Team in FCA wind tunnel

The four vertical struts, that fix the car to the platform, can change their height, to test several ride height maps (up to 30 heights in 20 minutes for each car configuration). The range for wheelbase and tracks positions can allow test from motorcycle to light commercial. Vertical struts can also be set in “floating” mode, removing any vertical bind and leaving the car to freely move in vertical direction, under the effect of aerodynamic lifting forces.

During our test, the four vertical struts were set in a fixed condition, so the setup of the car was constant during the whole test. Even though the floating mode is a more realistic condition, the fix mode was chosen because it is very challenging to emulate in CFD the movements that a race car has under the effect of its downforce. Furthermore, the central moving belt of the platform was less wide than the track of SC22. This kind of situation do not allow to calculate the real aerodynamic performance of the car, because a consistent part of the aerodynamic package (sidepods above all) is not “covered” by the belt. Nevertheless, the test has been very useful to validate our CFD model. As a result, yaw tests have not been conducted too.



Figure 4.2: Car fitting to the Rolling Road Simulation System

This test was conducted with almost constant pressure and temperature (and so density):

- $T \approx 25^{\circ}C$
- $p \approx 1.008 \cdot 10^5 Pa$
- $\rho \approx 1.18kg/m^3$ (*constant*)

The turbulence level at the inflow is low, (turbulence intensity equal to 0.1%).
The tests that have been carried out are:

- Reynolds sweep + pressure taps on the dorsal surface of the rear wing
 - Inflow velocity from 20 kph up to 100 kph (steps of 10 kph)
 - 16 pressure taps: 4 for main, 4 for the first flap, 5 for the second flap and 3 for the third one



Figure 4.3: Pressure taps on the rear wing

- Wake measurement
 - Inflow velocity fixed at 60 kph
 - 16 total pressure probes, spaced 6 cm one to another and connected to a rod. The rod was moved by the traversing gear shown in the figure on the side.

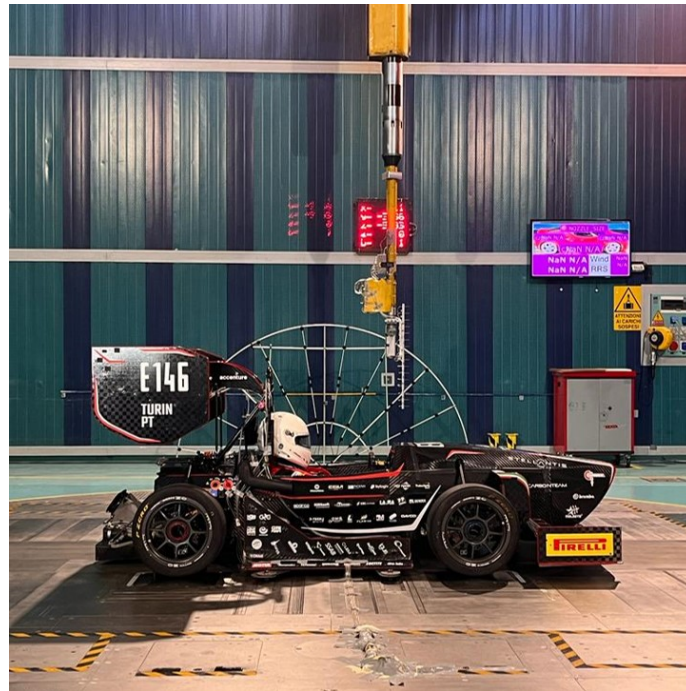


Figure 4.4: Wake measurement system

4.2 Flow Phenomenon

The main features of the test section was reproduced into the CFD model.

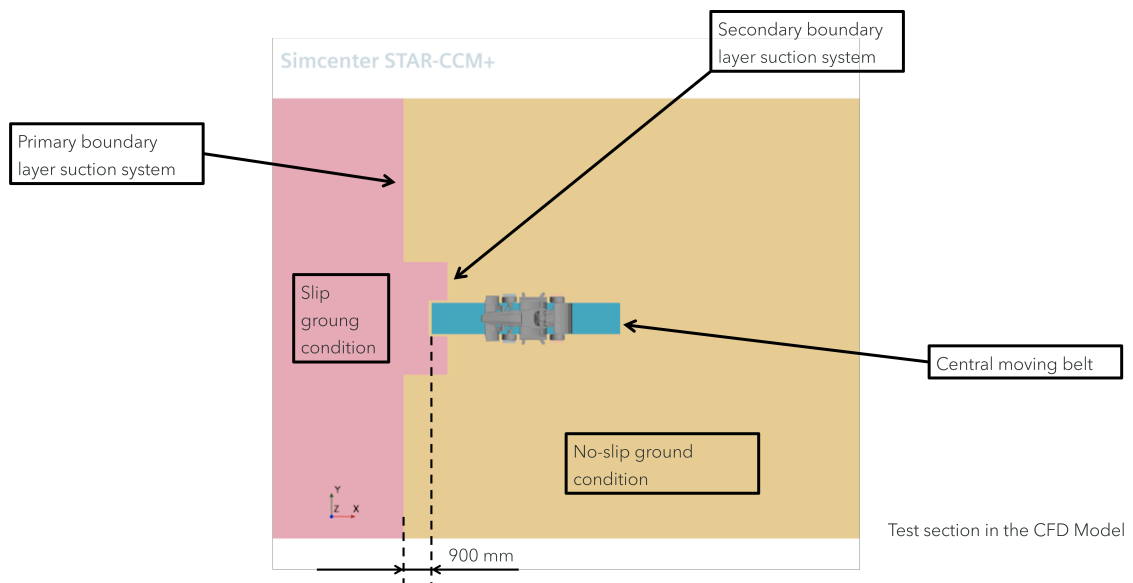


Figure 4.5: Test section in the CFD Model

The setup of the car was recreated in CAD too. That was possible thanks to the measurements taken about pitch and roll of the car, as well as toe and camber of the wheels.

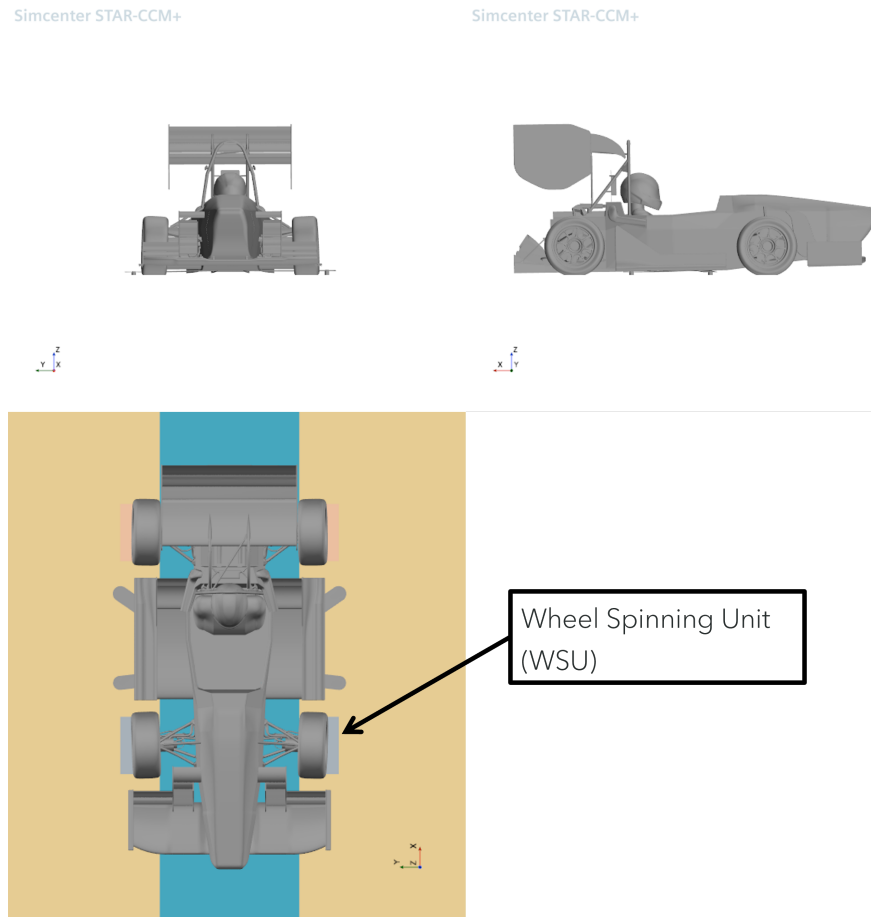


Figure 4.6: Car setup

The discretization of the domain was done by using the following two Meshers, available in STAR-CCM+

- Trimmed Cell Mesher for core cells
- Prism Layer Mesher to capture boundary layers near the walls. In general, an All- y^+ Wall Treatments was used, but for the ground a Low- y^+ Wall Treatment ($y^+ < 5$ almost on all ground surface) was preferred to capture precisely the atmospheric boundary layer in the wind tunnel test section.

As we were searching for steady-state solution, flow governing equations in the form of Reynolds-Averaged Navier-Stokes were solved with a Segregated Flow

approach. The closure of the problem was guaranteed by the SST (Menter) $k - \omega$ Turbulence Model.

Initial and boundary conditions were set case by case, depending on test conditions. In general, the conditions we controlled are:

- Air density $\rho \approx 1.18 \text{ kg/m}^3$ (constant)
- Air dynamic viscosity $\mu \approx 1.855 \cdot 10^{-5} \text{ Pa} \cdot \text{s}$ (constant)
- Inflow velocity variable with the test
- Outflow pressure equal to ambient pressure
- Turbulence intensity equal to 0.1% (constant)
- Turbulent Viscosity Ratio (TVR) ≈ 1 (constant)
- Turbulent Velocity Scale equal to the inflow velocity
- Central belt and WSU velocity equal to inflow velocity
- Angular speed for the rotating parts of the wheels.

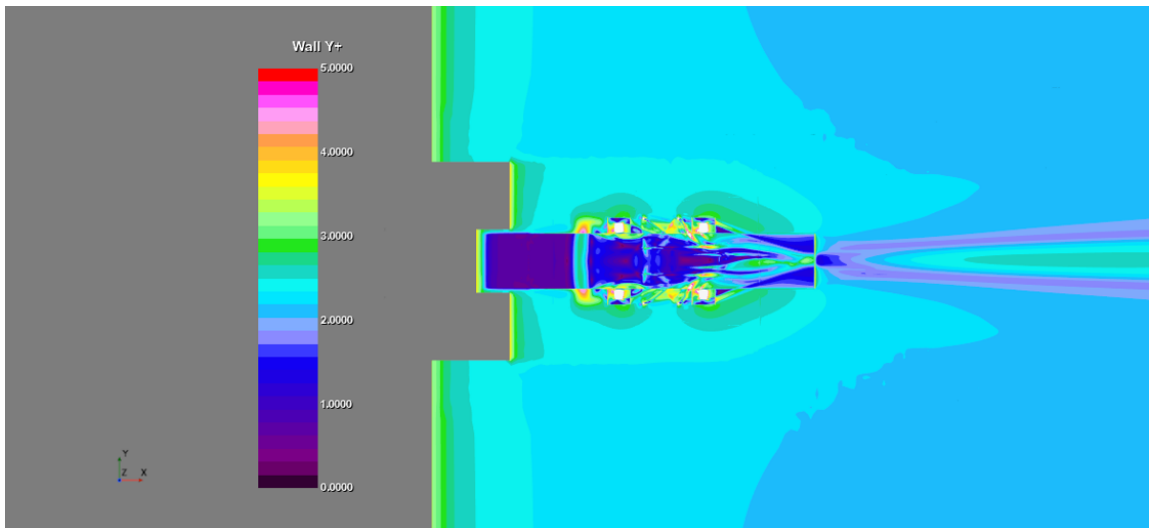


Figure 4.7: $y+$ in Wind Tunnel CFD Simulation

Chapter 5

Results and Discussion

In the previous chapters, I explored the theoretical foundations of CFD, the development of the numerical model and the complexities of the chosen validation case. In this chapter, I will present the end of the process, reveal the results of the simulations and engage in a rigorous discussion of the results.

The primary objective of this research was to validate the CFD model by comparing its predictions with experimental data obtained in the wind tunnel. Through careful analysis, the aim is to verify the accuracy and reliability of the simulations. The validation process is a key step in ensuring that CFD models can faithfully represent real-world fluid dynamic phenomena, thereby enhancing their usefulness in engineering, environmental science and various other fields.

This chapter is organised as follows: it begins with a presentation of the numerical results, including the pressure distributions. Next, I will engage in a detailed discussion of the results, highlighting both areas where the CFD model performed well and those where discrepancies with the experimental data were observed. I will analyse potential sources of error and assess the implications of these discrepancies for the wider applicability of the CFD model.

5.1 Data Analysis

The following data were obtained during the wake and static pressure measurements. The wake measurements were taken only for an inflow velocity of 60 kph, while the second ones were taken during a Reynolds sweep (inflow velocity from 40 kph up to 100 kph). Thus, for the 60 kph case (estimated car mean velocity) there are 2 measures, while for the other inflow velocities just the measure on the configurations with pressure taps.

The dataset comprises fundamental aerodynamic coefficients, C_x and C_z (normalized with respect to a frontal area of $1 m^2$), as well as aerodynamic efficiency and the distribution of aerodynamic loads.

In the post-processing stage, the relative errors between the results obtained from Computational Fluid Dynamics (CFD) simulations and Wind Tunnel experimentation has been calculated. These errors are denoted as ΔC_z , ΔC_x , and similar terms.

Inflow velocity 60 kph

- WT is the configuration with pressure taps on the rear wing.
- WT* is the configuration without pressure taps on the rear wing.

	C_z	C_x	C_z/C_x
WT	2.35	1.25	1.88
WT*	2.51	1.30	1.93
CFD	2.89	1.42	2.03

Table 5.1: Aerodynamics Coefficient 60kph

	ΔC_z	ΔC_z^*	ΔC_x	ΔC_x^*	$\Delta(C_z/C_x)$	$\Delta(C_z/C_x)^*$
CFD	23.12%	15.14%	13.95%	9.50%	8.05%	5.18%

Table 5.2: Delta Aerodynamics Coefficient 60kph

	%Front	%Rear
WT	52.8%	47.2%
WT*	49.8%	50.2%
CFD	43.3%	56.7%

Table 5.3: Aerodynamics Balance 60kph

The tables provided presents compelling evidence that the presence of pressure taps on the rear wing surface has a notable impact on the downforce generated by

the wing itself. Upon close examination, it becomes apparent that as these pressure taps are removed, there is a discernible increase in the coefficient of lift (C_z), indicating that the wing is producing more downforce. Moreover, a noteworthy shift occurs in the aerodynamic load distribution, transitioning from a "more Front" bias to a "more Rear" bias.

It is noteworthy that the data collected for the WT* configuration, particularly with the pressure taps in place, aligns more closely with the results obtained through Computational Fluid Dynamics (CFD) simulations. This is exemplified by a relative error on the coefficient of drag (C_x) of less than 13%, which is well within an acceptable range. While the error on the coefficient of lift (C_z) is somewhat higher, it remains within acceptable bounds. It is worth noting that C_z measurements are particularly influenced by underfloor aerodynamics, which, in turn, are significantly impacted by the Rolling Road Simulation System—a complex aspect that is challenging to replicate accurately in CFD simulations.

Moving to the subsequent tables, a fascinating trend emerges: the error between CFD results and Wind Tunnel data diminishes as airspeed increases. This finding suggests that higher airspeeds enhance the reliability of wind tunnel measurements. This phenomenon can be attributed to the fact that at higher velocities, the flow conditions more closely mimic real-world scenarios, resulting in a closer alignment between experimental and computational data.

In summary, the data presented underscores the significance of pressure taps on the rear wing's aerodynamic performance, revealing a substantial impact on downforce and load distribution. Additionally, the correlation between WT* configuration data and CFD results highlights the importance of accurate simulation and measurement techniques in the field of aerodynamics. Finally, the observed trend of reduced error at higher airspeeds underscores the relevance of testing conditions and their impact on data reliability in the context of aerodynamic research and development.

Inflow velocity 40 kph. Pressure taps on the rear wing

	C_z	C_x	C_z/C_x	ΔC_z	ΔC_x	$\Delta(C_z/C_x)$
WT	2.29	1.20	1.91			
CFD	2.97	1.55	1.92	29.66%	28.75%	0.71%

Table 5.4: Aerodynamics Coefficient and Delta 40kph

	%Front	%Rear
WT	49.6%	50.4%
CFD	39.9%	60.1%

Table 5.5: Aerodynamics Balance 40kph

Inflow velocity 80 kph. Pressure taps on the rear wing

	Cz	Cx	Cz/Cx	ΔC_z	ΔC_x	$\Delta(C_z/C_x)$
WT	2.37	1.23	1.92			
CFD	2.87	1.38	2.08	21.20%	12.32%	7.90%

Table 5.6: Aerodynamics Coefficient and Delta 80kph

	%Front	%Rear
WT	54.0%	46.0%
CFD	44.6%	55.4%

Table 5.7: Aerodynamics Balance 80kph

Inflow velocity 100 kph. Pressure taps on the rear wing

	Cz	Cx	Cz/Cx	ΔC_z	ΔC_x	$\Delta(C_z/C_x)$
WT	2.40	1.22	1.96			
CFD	2.85	1.37	2.08	19.04%	12.27%	6.04%

Table 5.8: Aerodynamics Coefficient and Delta 100kph

	%Front	%Rear
WT	55.0%	45.0%
CFD	45.0%	55.0%

Table 5.9: Aerodynamics Balance 100kph

Pressure Coefficient Measurements

The study in question pertains to an investigation involving Reynolds sweep, combined with the strategic placement of pressure taps on the dorsal surface of the Rear Wing (RW). This study aims to explore the aerodynamic behavior of the rear wing under varying inflow velocities, ranging from 20 kph to 100 kph, with incremental steps of 10 kph.

To ensure comprehensive data collection, a total of 16 pressure taps have been strategically positioned on the rear wing. These pressure taps are thoughtfully distributed to capture essential information across different regions of the wing's structure. Specifically, there are four pressure taps dedicated to the main wing section, another four allocated to the first flap, five serving the second flap, and three focusing on the third flap. These pressure taps are carefully collocated at a fixed distance of $Y = 306$ millimeters from the centerline of the car.

This experimental setup is designed to provide a thorough understanding of how the rear wing's aerodynamic characteristics evolve as a function of both inflow velocity and its intricate geometry. By incorporating the Reynolds sweep methodology, which considers the variation of flow conditions, and the precise placement of pressure taps, the study aims to yield highly detailed and informative data.

The investigation's range of inflow velocities, spanning from 20 kph to 100 kph, is chosen deliberately to encompass a broad spectrum of real-world driving conditions. These velocity increments of 10 kph allow for a systematic exploration of the wing's performance across various speed regimes, enabling researchers to observe any notable trends or dependencies in the aerodynamic behavior.

The figure below offers a visual representation of the pressure coefficient distribution for a specific inflow velocity of 60 kilometers per hour (kph). In this plot, two distinct curves are depicted: a black distribution, which represents the pressure coefficient distribution fully derived from Computational Fluid Dynamics (CFD) simulations, and a red curve, which was generated through the interpolation of experimental data collected by pressure taps.

As elucidated in the preceding section, it is important to recognize that the experimental measurements obtained through pressure taps may be influenced by the presence of these measurement devices themselves. To address this potential source of error, a meticulous correction process was employed. This correction was executed by utilizing data obtained from wake measurement tests conducted at the same velocity. The inclusion of this correction factor, represented by the blue line

in the plot, helps refine the accuracy of the experimental data by accounting for any distortions introduced by the pressure taps.

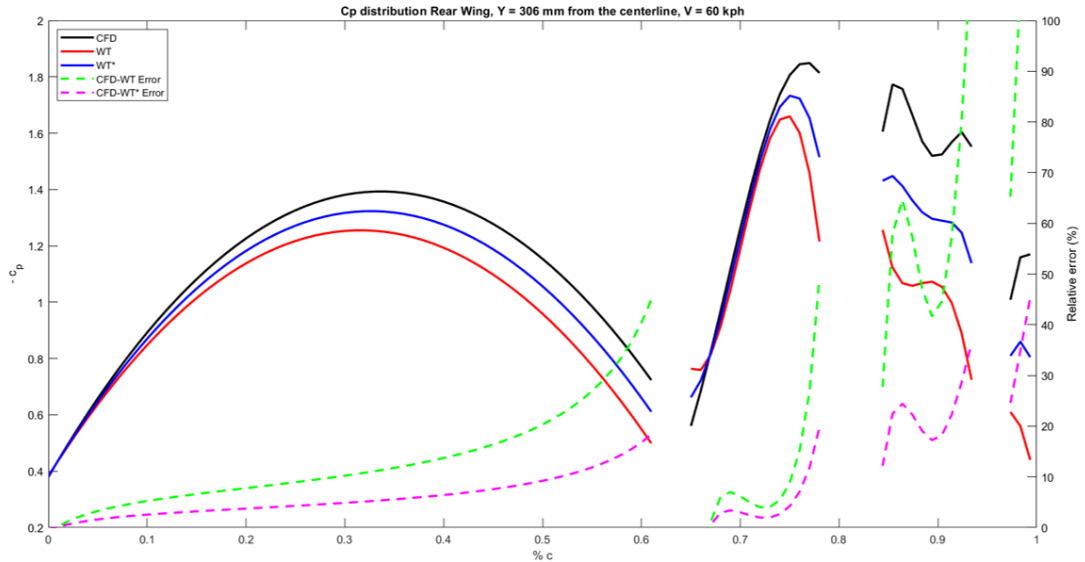


Figure 5.1: Pressure Coefficient on Rear Wing, Y=306 mm

The correction factor in question was determined following a meticulous analysis of data derived from a series of simulations conducted at a velocity of 60 kph, both with and without the incorporation of pressure taps. Examining the results presented in Table 5.1, a noteworthy observation emerges: the coefficient of lift (C_z) undergoes a discernible alteration, ranging from 2.35 to 2.51 when comparing the scenarios with and without pressure taps. This alteration is accompanied by a significant shift in the vehicle's balance toward the rear.

From this, it is reasonable to infer that the load variation is primarily attributable to the presence of pressure taps, suggesting that the entirety of this effect is concentrated on the rear wing. Consequently, we can surmise that the pressure taps are exerting a considerable influence on the rear wing's performance.

Moreover, another key assumption made in this analysis is the constancy of the coefficient of pressure (C_p) across the entire chord length of interest. This assumption facilitates the calculation of an average C_p value by leveraging the obtained ΔC_z values. This calculated average C_p can then be subtracted from the C_p values acquired through measurements at specific points using the pressure taps within the wind tunnel. This approach streamlines the analysis and interpretation of the data, allowing for more insightful insights into the aerodynamic characteristics of the vehicle under consideration.

Notably, the plot serves to underscore a critical observation made during the data analysis phase. It reiterates that CFD estimations consistently yield higher values for aerodynamic load in comparison to the measurements acquired in the wind tunnel. This discrepancy between CFD predictions and experimental data has been a recurrent finding throughout the study, indicating that there may be inherent differences between the computational modeling approach and the real-world conditions encountered in the wind tunnel.

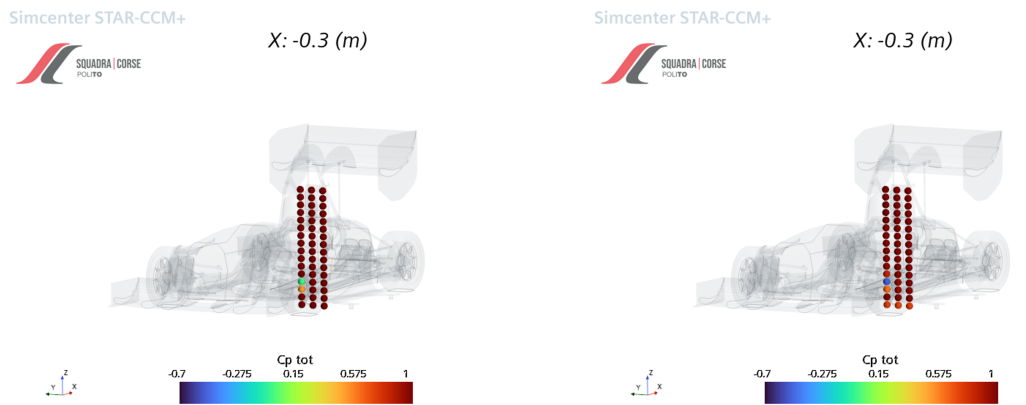


Figure 5.2: Wake measurement 1

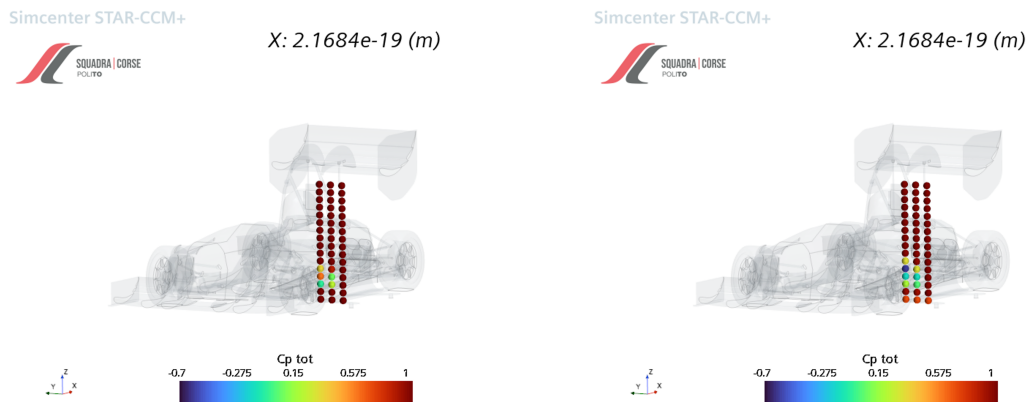


Figure 5.3: Wake measurement 2

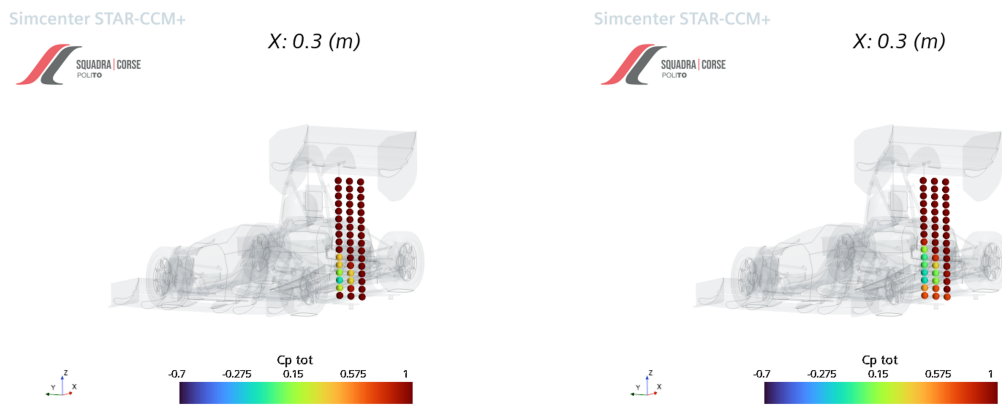


Figure 5.4: Wake measurement 3

These first three images represent the wake measurement behind the wheel and near the sidepod. A very complicated area from an aerodynamic point of view as the behaviour of a tyre and its wake is one of the most difficult phenomena to simulate from a CFD point of view. It can be seen that despite some divergence from a numerical point of view, the shape of the two wakes is very similar.

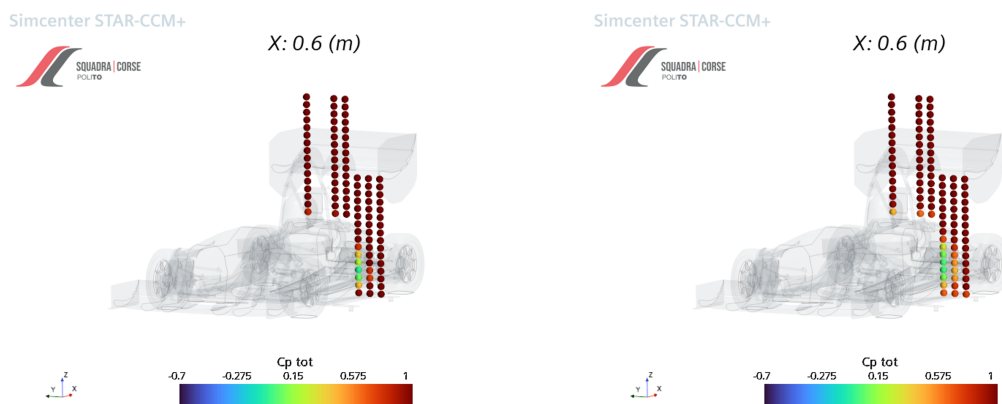


Figure 5.5: Wake measurement 4

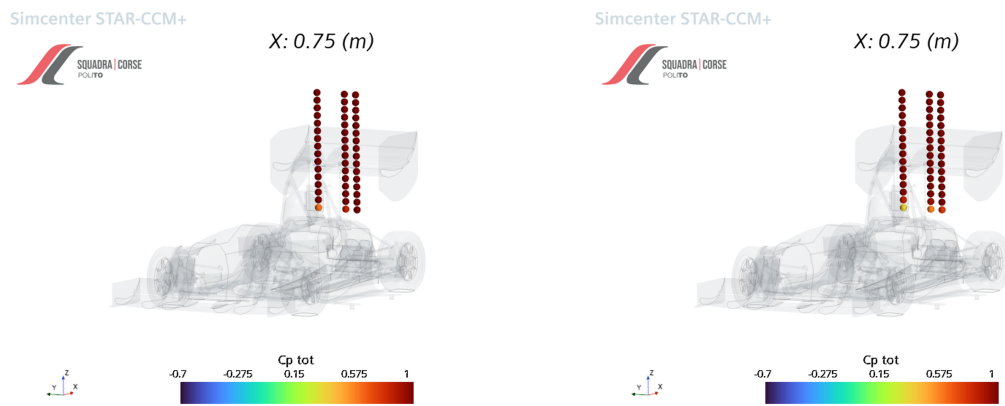


Figure 5.6: Wake measurement 5

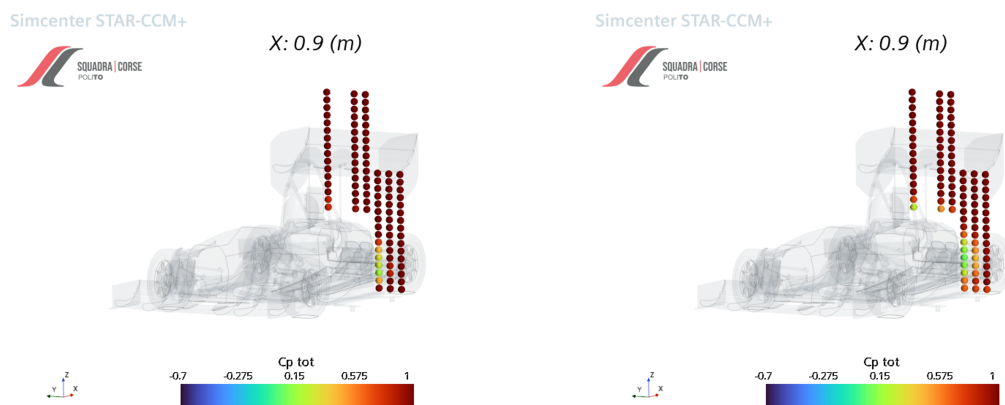


Figure 5.7: Wake measurement 6

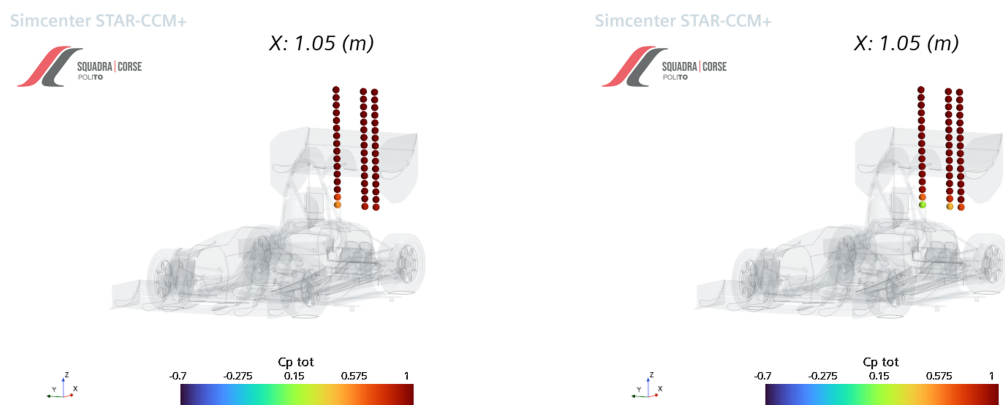


Figure 5.8: Wake measurement 7

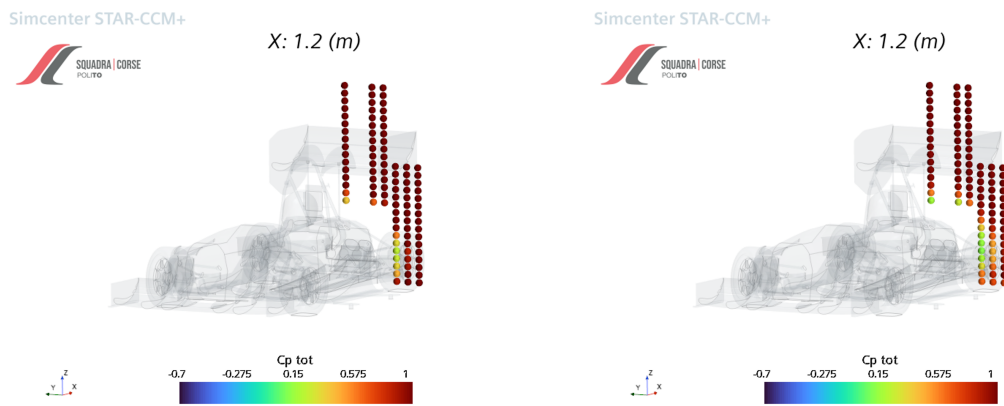


Figure 5.9: Wake measurement 8

Instead, these images show the wake measurements above and near the sidepod, an area of particular interest due to the software's difficulty in meshing a high-quality mesh due to the complexity of the geometry. Again, we can be satisfied with the results obtained.

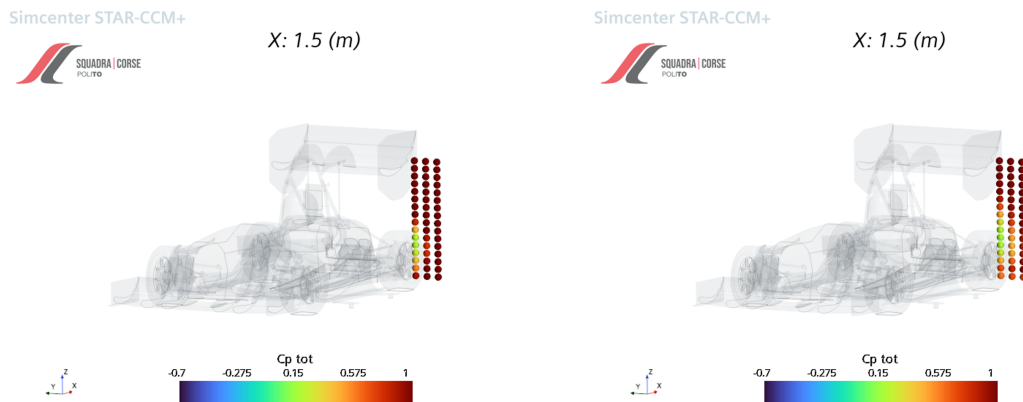


Figure 5.10: Wake measurement 9

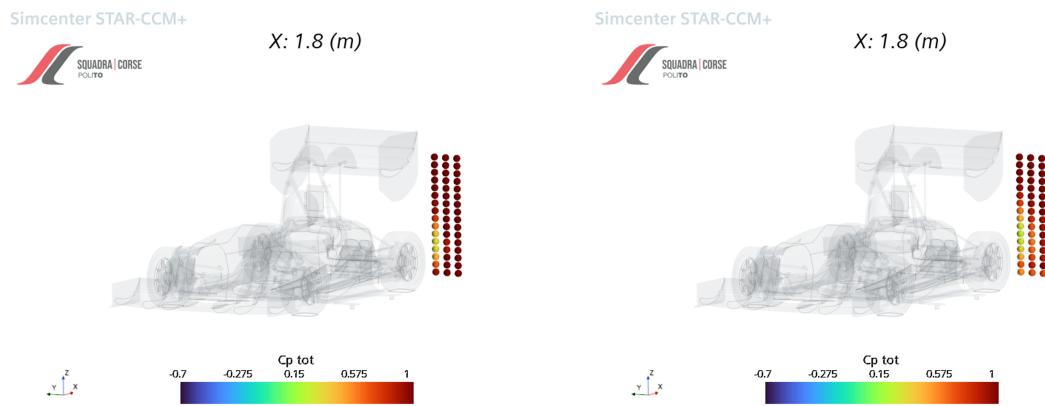


Figure 5.11: Wake measurement 10

As with the front wheel wake, a measurement of the total pressure coefficient was carried out for the rear wheels. In this case, in addition to the slight discrepancy in numbers, it can be seen that the wake measured in the tunnel is slightly wider than that calculated by simulation.

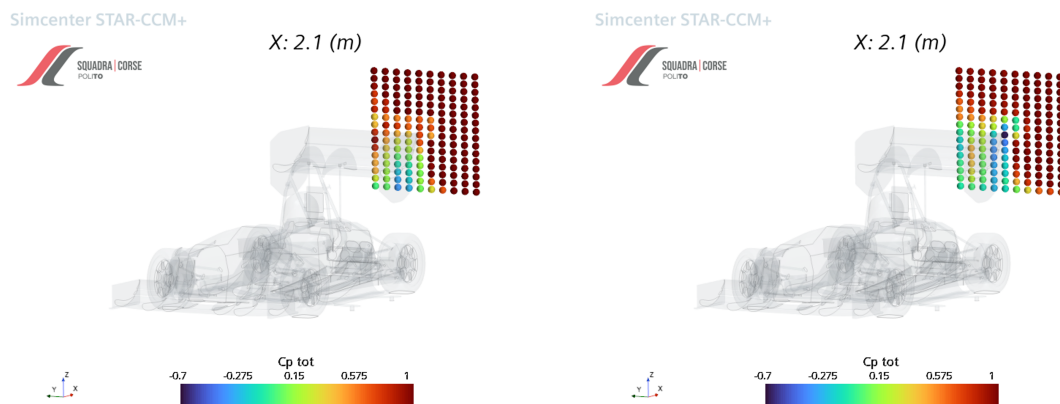


Figure 5.12: Wake measurement 11

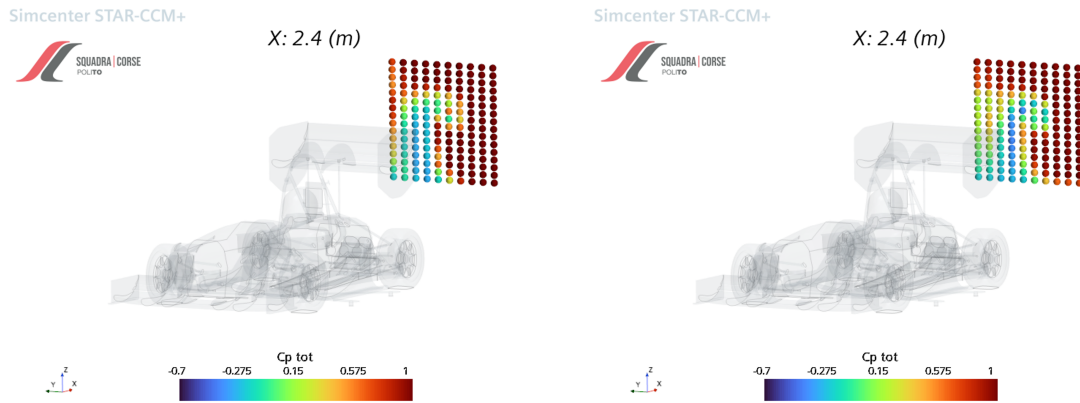


Figure 5.13: Wake measurement 12

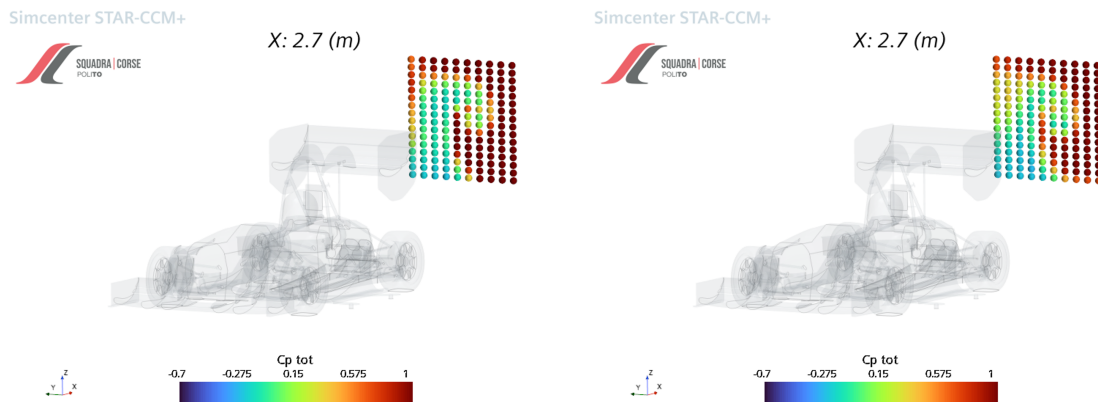


Figure 5.14: Wake measurement 13

In the closing stages of the experiment, a comprehensive assessment of the wake trailing the vehicle is conducted. An intriguing observation emerges: the configuration of the wake recorded in the wind tunnel closely parallels the one computed through the simulations. This alignment between empirical observations and computational forecasts signifies a significant concurrence in the aerodynamic behavior of the vehicle across these two distinct testing environments.

Notably, the accord extends to the vortex region positioned at the wake's tip. The wind tunnel data adeptly replicates the shape of this vortex area, demonstrating a high degree of precision. While some marginal disparities in vortex intensity exist when comparing the experimental and simulated outcomes, it's noteworthy that a detailed clarification for these differences will be presented in the upcoming section.

The preceding figures have illuminated several noteworthy observations and insights: first and foremost, there exists a commendable level of correlation between the total pressure probes strategically positioned on the sides of the car. This correlation is of significant importance as it pertains to one of the most critical regions within the flow field surrounding the car. The area around the sides of the car, particularly in close proximity to the tires, presents a particularly challenging environment for accurate measurement and analysis. Modern Computational Fluid Dynamics (CFD) codes, while highly advanced, still grapple with the intricacies of capturing the intricate flow patterns created by the wake of the tires. In this context, the fact that the total pressure probes demonstrate good alignment in their readings signifies a valuable aspect of the study's data reliability.

Furthermore, it is worth noting that the wind tunnel car model used in this investigation featured lateral bars designed to secure the vehicle to the vertical struts within the tunnel. These bars, while essential for maintaining the car's stability during testing, introduce an additional element into the aerodynamic equation: turbulence. The presence of these lateral bars generates turbulence in the airflow around the car, further complicating the flow field and making precise measurements all the more challenging.

5.2 Sources of Discrepancy

The source of the discrepancy between computational fluid dynamics (CFD) simulations using the k-omega SST turbulence model and wind tunnel experiments can be attributed to several key factors.

Firstly, one major factor is the inherent simplifications and assumptions made in the CFD modeling process. CFD simulations are based on numerical discretization of the governing equations, and they require numerous simplifications to make the calculations computationally feasible. These simplifications can lead to inaccuracies, especially in capturing complex turbulent flow phenomena that may occur in a real-world wind tunnel.

Secondly, the k-omega SST turbulence model itself has limitations. It is a two-equation turbulence model that combines the k-omega and k-epsilon models to provide better predictions for a wide range of flow scenarios. However, it still relies on certain assumptions about the turbulence characteristics, and its performance may degrade when applied to flows with unique features or extreme conditions that deviate from its underlying assumptions.

Thirdly, geometry representation in CFD simulations may not perfectly replicate the real-world wind tunnel setup. Modeling complex geometries with high fidelity in CFD can be challenging and may introduce errors. It should be emphasised here that the setup to place the car in the wind tunnel was not optimal. The ground clearance was not very precise and the car being very sensitive to heights above the ground, even by a few millimetres, may certainly have influenced the results. By changing these heights and the pitch of the car, you can get more or less similar results to those in the wind tunnel. Another factor that influenced the results is the roll the car had during the tests. One aspect that certainly needs to be improved for future wind tunnel simulations is precisely this. You have to be sure of the height, pitch, camber and toe of the car.

Fourthly, the numerical discretization and grid resolution in CFD simulations can have a substantial impact on the accuracy of the results. Insufficient grid resolution or poor mesh quality can lead to numerical artifacts and may not capture the fine details of the flow field observed in the wind tunnel.

Lastly, uncertainties in the experimental data obtained from the wind tunnel itself can contribute to the observed discrepancies. Wind tunnel measurements are subject to experimental errors and uncertainties in instrument calibration, data acquisition, and post-processing, which can introduce variations in the results.

In summary, the differences between CFD simulations using the k-omega SST turbulence model and wind tunnel experiments can be attributed to the inherent limitations and simplifications in CFD, the specific characteristics of the turbulence model, boundary condition discrepancies, grid resolution issues, and experimental uncertainties in the wind tunnel data. These factors collectively contribute to the observed deviations between the two approaches in studying fluid flow phenomena.

Indeed, despite the multifaceted sources of discrepancy outlined, it is noteworthy that the results obtained through computational fluid dynamics (CFD) simulations employing the k-omega SST turbulence model exhibit a remarkably high level of agreement with the experimental data acquired from wind tunnel measurements, particularly in the context of wake measurements. The convergence of CFD and wind tunnel results within the realm of the pressure field is striking, underscoring the model's capacity to accurately reflect the intricacies of the flow phenomena observed within the controlled environment of the wind tunnel.

One particularly promising aspect of this alignment is the remarkable consistency in the pressure field representations, where the CFD model effectively mirrors the pressure patterns measured in the wind tunnel. The level of agreement in

this critical aspect of the analysis is a testament to the model's ability to capture the underlying physics governing the flow, even amidst the complex turbulence characteristics inherent to such scenarios.

Furthermore, it is essential to emphasize that the observed differences between CFD and wind tunnel results, while present, are relatively modest in magnitude, typically amounting to only a few percentage points. This degree of proximity between the model and experimental outcomes provides strong evidence in favor of the model's credibility and its capacity to serve as a reliable predictive tool for understanding and simulating real-world fluid flow phenomena.

In light of these compelling findings, it is plausible to conclude that the CFD model, underpinned by the k-omega SST turbulence model, has achieved a level of validation that can instill confidence in its ability to faithfully represent the underlying reality of the flow scenario in question. The convergence of results and the minor differentials observed between simulations and experiments not only underscore the robustness of the model but also suggest that it serves as a valuable and practical tool for investigating and understanding the intricate dynamics of fluid flow in the context of the specific wind tunnel experiments under consideration.

Chapter 6

Aerodynamic Maps and Cornering Simulations

This chapter unfolds in two distinct parts: the first part focuses on an exhaustive examination of the current state of AeroMaps specific to Formula Student vehicles, while the second part delves into the evolution of these maps, with a particular emphasis on incorporating cornering situations.

The first part of this chapter is dedicated to providing an in-depth analysis of the existing AeroMaps that have influenced the design and performance of the vehicle. The landscape of Formula Student engineering is one of constant innovation and evolution. As these student-designed vehicles continue to push the limits of performance and agility, it becomes increasingly crucial to expand our understanding of their aerodynamic behavior, particularly when subjected to the complex dynamics of cornering. Therefore, the second part of this chapter shifts its focus towards the evolution of AeroMaps, emphasizing the integration of cornering situations into the design process.

6.1 Ride Height Aero Map

An aero map provides a graphical representation of how a racecar's aerodynamic characteristics, including lift, drag, and balance, change in response to specific adjustments made to the car's setup. This map illustrates how altering factors like the car's front and rear ride heights or the angle of the rear wing directly impact its aerodynamic performance. In essence, it offers a visual roadmap for understanding how geometric changes influence the way a racecar interacts with the air.

For the model geometry limits are imposed by suspensions' excursion:

- Front Height: 5 mm-55 mm from the ground
- Rear Height: 5 mm-55 mm from the ground

Each configuration is achieved translating all the suspended masses and then rotating around the front-wheels axis

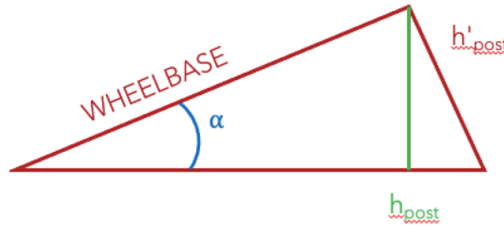


Figure 6.1: Geometry Setup

$$h_{post} \approx h_{post} (\alpha \text{small}) \quad (6.1)$$

$$\frac{h_{post}}{\sin\alpha} = \text{wheelbase} \quad (6.2)$$

$$\alpha = \arcsin\left(\frac{h_{post}}{\text{wheelbase}}\right) \quad (6.3)$$

The heights have been organized into a 7x7 matrix, as shown in the table. This matrix strikes a balance between the level of detail or resolution required and the number of simulations that need to be conducted. It's worth noting that some of the red configurations encountered issues with ground interference, making them unworkable during the initial simulations. However, we were able to extrapolate data from these configurations in the post-processing phase.

The model was prepared by means of the basic simulation model and the use of the **DFM** function (ANSA) was used, in order to save time with CAD-export.

- Green: rotated/translated parts
- Violet: morphed parts (suspensions and cables)
- Blue: fixed parts (wheel group)

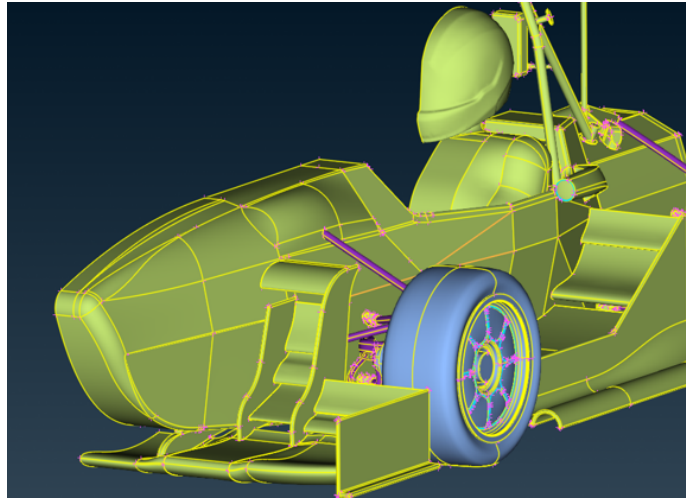


Figure 6.2: DFM Function ANSA

A 7x7 matrix was obtained for the following quantities:

- C_z
- C_x
- Front repartion (%)
- Rear repartition (%)

This data will be integrated in Vehicle Dynamics simulation-model.

Cz							
	5	15	25	30	35	45	55
5	3.34	3.18	3.09	3.12	3.73	3.28	3.23
15	3.68	3.67	4.48	4.50	4.21	3.96	3.47
25	4.71	4.71	4.72	4.64	4.56	4.38	4.18
30	4.68	4.73	4.77	4.73	4.65	4.49	4.33
35	4.63	4.67	4.71	4.67	4.62	4.54	4.40
45	4.46	4.52	4.57	4.52	4.46	4.38	4.28
55	4.51	4.43	4.36	4.32	4.29	4.23	4.13

Figure 6.3: Ride Height Table

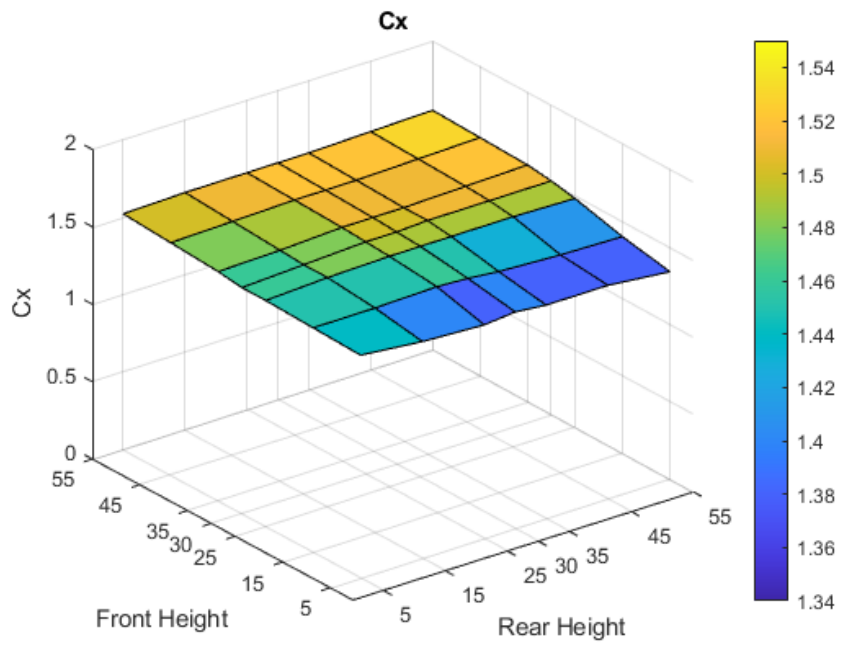


Figure 6.4: AeroMap C_x

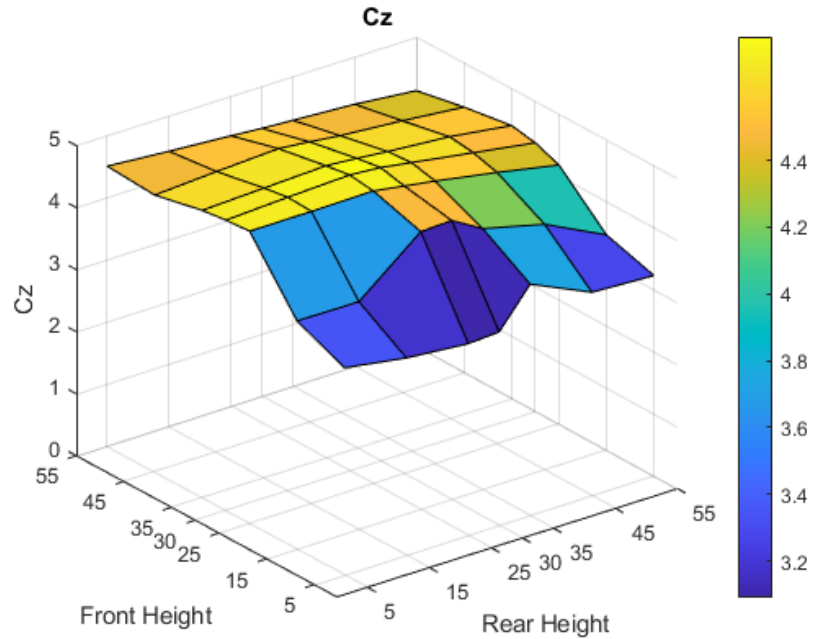


Figure 6.5: AeroMap C_z

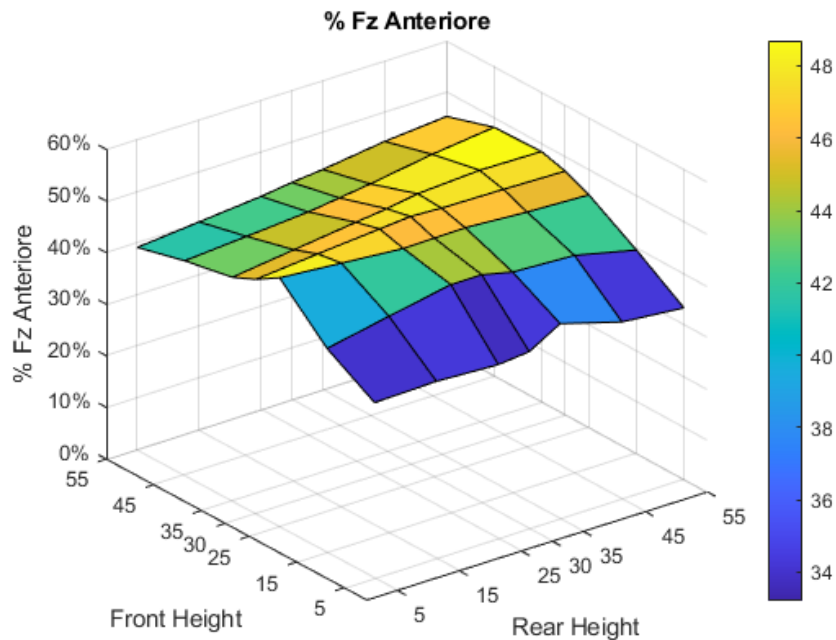


Figure 6.6: AeroMap Aerobalance

6.2 Skidpad Cornering Simulation

The Skidpad event in Formula SAE (Society of Automotive Engineers) is a dynamic handling test designed to evaluate a race car's lateral grip and handling characteristics. It is one of the dynamic events that teams competing in Formula SAE competitions must participate in. The Skidpad event tests a car's ability to navigate a circular track while maintaining a constant radius and high lateral acceleration. Here's an explanation of the Skidpad event formula and how it works:

- **The Skidpad Track:** The Skidpad event typically takes place on a circular track marked with cones. The radius of this circular track is predetermined by the competition organizers. The track surface is usually smooth to ensure consistent testing conditions.
- **Objective:** The objective of the Skidpad event is to measure the maximum lateral acceleration that a Formula SAE car can achieve while going around the circular track without losing traction (i.e., without skidding). This test helps evaluate the car's cornering performance, tire grip, and overall handling balance.
- **Challenges:** The Skidpad event challenges teams to optimize their car's suspension geometry, aerodynamics, and tire selection to maximize lateral grip

while maintaining stability. Teams need to balance factors like tire selection, tire pressure, and suspension setup to achieve the best results.

- **Importance:** The Skidpad event is crucial because it assesses a car's ability to handle corners effectively, which is a fundamental aspect of racing performance. It also showcases a team's engineering and design capabilities in optimizing the vehicle's dynamics.

In summary, the Skidpad event in Formula SAE is a test of a race car's ability to maintain traction and navigate a circular track at a constant radius while experiencing high lateral acceleration. It assesses the car's handling and grip characteristics and is an important component of the overall competition, which evaluates the engineering prowess of student-designed and built race cars.

For the simulation some data are needed and they are derived from the log file of the Skidpad event. The data are:

- X-Position of CoG
- Angle and angular speed of each tyre
- Geometry of suspension
- Roll angle

Another important feature in these simulations is Side Slip Angle β which is defined positive if counterclockwise (6.7). A precise evaluation of this angle is difficult and expensive, but a realistic attempt range can be $[-5^\circ; +5^\circ]$.

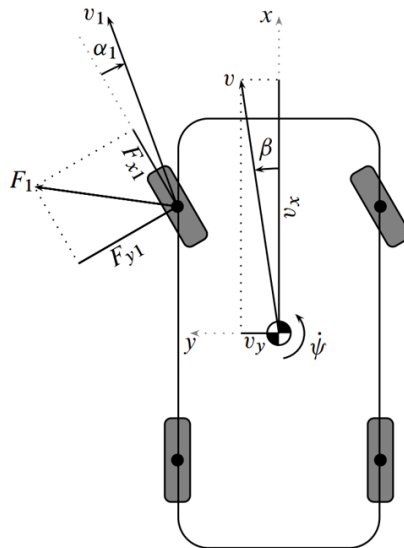


Figure 6.7: Side Slip Angle definition

6.2.1 Simulation setup

Domain

An approach for the calculation domain has been studied by Siemens, so the parameters and measures of the domain have been obtained starting from this study. [8]

The study was conducted for two cornering radius, so the resulting data was linearly interpolated obtaining:

- $R_{out} = 1.3R + 39$ [m]
- $\alpha_{in} = \frac{m \cdot Wheelbase}{R} \frac{180}{\pi}$ [deg]
- $\beta_{out} = \frac{2m \cdot Wheelbase}{R} \frac{180}{\pi}$ [deg]
- $m = 0.9412R + 1.1176$ [rad]
- $H = 16$ [m]

where R parameter was taken highest as possible, so if it will result in a too high number of cells, it can be reduced.

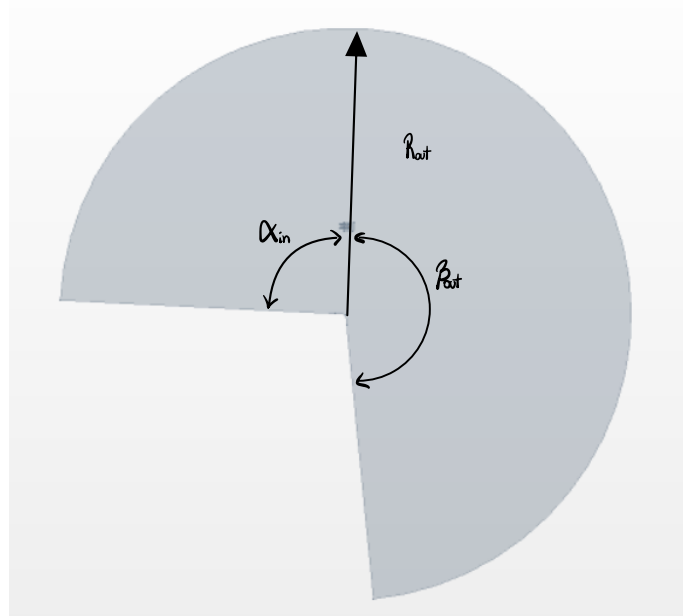


Figure 6.8: Construction of the Skidpad domain

The domain has been designed using CATIA V5 in a parametric way and then imported on star ccm+.

Refinement Boxes

Wake Refinement boxes have been created with CATIA V5, as for the domain construction in a parametric way in order to simply modify it in case of need, using the following 6 sections:

Section	Width Definition [m]	Height Definition [m]	Angle From Prior Section
1	2.5	2	$0.45 * WB/R$
2	$2.5 + 3.5/(OAW - 0.45) * 4$	$2 + 2.5/(OAW - 0.45) * 4$	$4 * WB/R$
3	$2.5 + 3.5/(OAW - 0.45) * 8.5$	$2 + 2.5/(OAW - 0.45) * 8.5$	$4 * WB/R$
4	$2.5 + 3.5/(OAW - 0.45) * (8.5 + 0.25 * OAW)$	$2 + 2.5/(OAW - 0.45) * (8.5 + 0.25 * OAW)$	$4 * WB/R$
5	$2.5 + 3.5/(OAW - 0.45) * (8.5 + 0.5 * OAW) * 4$	$2 + 2.5/(OAW - 0.45) * (8.5 + 0.5 * OAW)$	$0.25 * OAW * WB/R$
6	6	4.5	$(0.5 * OAW - 8.95) * WB/R$

Table 6.1: Definition of sketches for the refinement boxes [9]

where OAW stands for Outlet Angle Wheelbase.

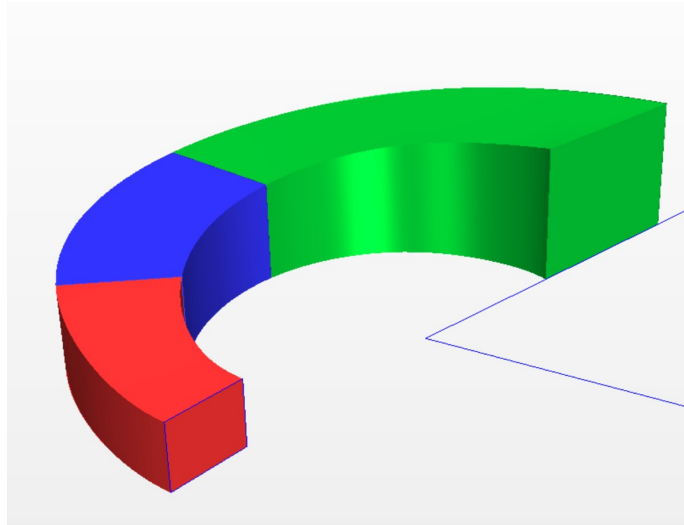


Figure 6.9: Refinement Boxes [9]

Boundary conditions

Boundary conditions, have to be redefined for this type of simulation, and they are resumed in 6.10.

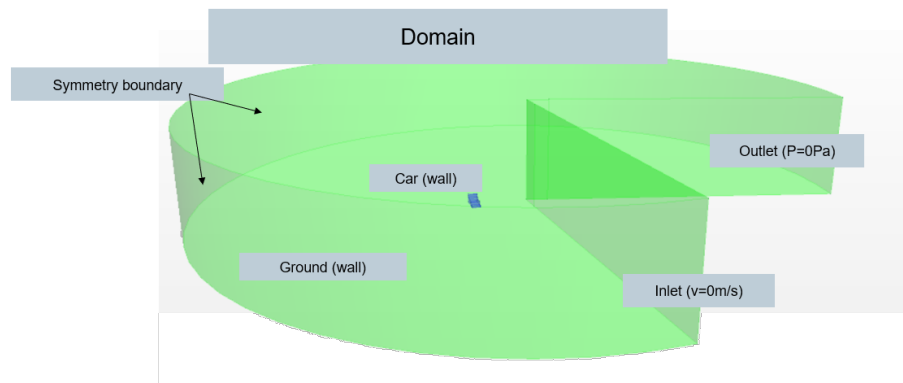


Figure 6.10: Scheme of Boundary Conditions

Additionally:

- A Moving reference frame centered in the Center of Rotation (CoR) of the vehicle will be defined, with angular speed ω
- The MRFs reference frames will be redefined as a rotating reference frame inside the whole rotating reference frame
- All the regions (including radiators, BP, ecc) will be assigned to the whole rotating reference frame
- The ground will be a wall without relative speed
- For the walls both Symmetry boundary or Slip condition can be used.

6.3 Derivatives of Aerodynamic Coefficients

In order to have a more complete aerodynamic maps and not only the one that takes into account the pitch motion, a CFD model for the cornering situation is needed. Cornering motion can be decomposed into yaw and sideslip motions. Then, thanks to a study of Aerodynamics Evaluation of Road Vehicles in Dynamic Maneuvering, we assumed that the aerodynamic side force and yaw moment of a cornering motion could be expressed by superposing linear expressions of yaw motion parameters and those of sideslip motion parameters, respectively. [10].

First, a linear model to describe aerodynamic forces is needed. In this model, we took into account how aerodynamic properties change with both yaw motion and sideslip motion. Specifically, we hypothesized that the coefficients for side force

(C_s) and yaw moment (C_{YM}) could be defined as functions of several variables: the yaw velocity (r), sideslip angle (β), yaw acceleration (\dot{r}), and sideslip angle change in time($\dot{\beta}$).

$$C_s = C_s(r, \beta, \dot{r}, \dot{\beta}) \quad (6.4)$$

$$C_{YM} = C_{YM}(r, \beta, \dot{r}, \dot{\beta}) \quad (6.5)$$

Then the assumption that these coefficient could be expressed by linearly superposing Taylor expansion of each motion parameter is done. The other assumption is that the effects of the 2nd order and higher-order term of each motion parameters are minimal. So we have:

- Unsteady model of side force coefficient

$$C_s(r, \beta, \dot{r}, \dot{\beta}) = Y_r r + Y_\beta \beta + Y_{\dot{r}} \dot{r} + Y_{\dot{\beta}} \dot{\beta} + C_{s,0} \quad (6.6)$$

- Unsteady model of yaw moment coefficient

$$C_{YM}(r, \beta, \dot{r}, \dot{\beta}) = N_r r + N_\beta \beta + N_{\dot{r}} \dot{r} + N_{\dot{\beta}} \dot{\beta} + C_{YM,0} \quad (6.7)$$

Here, $Y_r, Y_v, Y_{\dot{r}}, Y_{\dot{v}}$ are 1st-order aerodynamic derivatives of each motion parameters for side force coefficient, and $C_{S,0}$ is constant term. $N_r, N_v, N_{\dot{r}}, N_{\dot{v}}$ are 1st-order aerodynamic derivatives of each of the motion parameters for the yaw moment coefficient, and $C_{YM,0}$ is a constant term.

For the quasi-steady model we have:

- Quasi-steady model of side force coefficient

$$C_s(r, \beta) = Y_r r + Y_\beta \beta + C_{s,0} \quad (6.8)$$

- Quasi-steady model of yaw moment coefficient

$$C_{YM}(r, \beta) = N_r r + N_\beta \beta + C_{YM,0} \quad (6.9)$$

The findings presented in the paper reveal a noteworthy convergence between the side coefficient curves obtained from a transient simulation and those derived from the quasi-steady linear model, particularly within the linear region. This observed alignment of results suggests a high degree of overlap and agreement between the two approaches. Consequently, we can confidently assert that the linear model serves as an effective and reliable methodology for constructing aerodynamic

maps that accurately incorporate the influence of cornering maneuvers. In other words, it demonstrates that the linear model is a robust tool for characterizing the aerodynamic behavior during cornering maneuvers, thereby enhancing our ability to model and predict the aerodynamic forces and moments involved in such maneuvers with a high level of accuracy.

In the process of constructing these aerodynamic maps, we employ two distinct models. The first of these is the yaw motion model, which shares similarities with the one utilized for the Skidpad analysis. This model is adept at capturing the dynamic behavior of the vehicle during yawing motions, enabling us to comprehensively understand and characterize its response under such conditions. On the other hand, the sideslip model takes a somewhat different approach. It draws inspiration from the symmetry model, but with a notable distinction—the vehicle under consideration is fully assembled and assumes a specific sideslip angle. This departure from the classic symmetry model accounts for the practical realities of a complete vehicle and allows us to factor in the effects of sideslip, thus enhancing the model's fidelity in representing real-world scenarios.

By employing these two distinct yet complementary models, we are better equipped to develop comprehensive and accurate aerodynamic maps that can effectively account for the nuances of yaw motion and sideslip, providing a more robust foundation for understanding and predicting the vehicle's aerodynamic behavior during complex maneuvers.

6.4 Yaw rate Simulation

In this section, the results of simulations at varying yaw rates are presented. The CFD model used is the same as that used for the Skidpad simulations but with zero beta angle, roll angle and pitch angle. The only parameter that varies in the simulations is the yaw rate. In particular, since yaw is proportional to speed and cornering radius, the parameter that changes in these simulations is speed. Simulations were also carried out where the speed remained constant and the parameter that varied was the cornering radius. The results were identical to those where the changing parameter was the speed.

The aerodynamic derivatives Y_r and N_r are determined as coefficients that represent the proportional relationship between the side force and yaw moment coefficients and the yaw rate. The constant terms $C_{s,r}$ and $C_{YM,r}$ are obtained from CFD analyses and represent the fixed values in these equations.

Yaw rate r [rad/s]	Velocity [km/h]	a_c	C_z	C_s	C_{YM}
1.009	34.088	1.02 g	-4.756	-0.0009	0.078
1.184	40	1.34 g	-4.742	-0.0262	0.006
1.303	44	1.62 g	-4.658	-0.0503	0.002

Table 6.2: Yaw rate Table Coefficient

Thanks to the "Curve Fitting" tool of Matlab a linear regression was calculated and the following results were derived :

- $Y_r = 0.08062$ [s/rad]
- $N_r = 0.116$ [s/rad]
- $C_{s,r} = -0.3012$
- $C_{YM,r} = -0.6265$

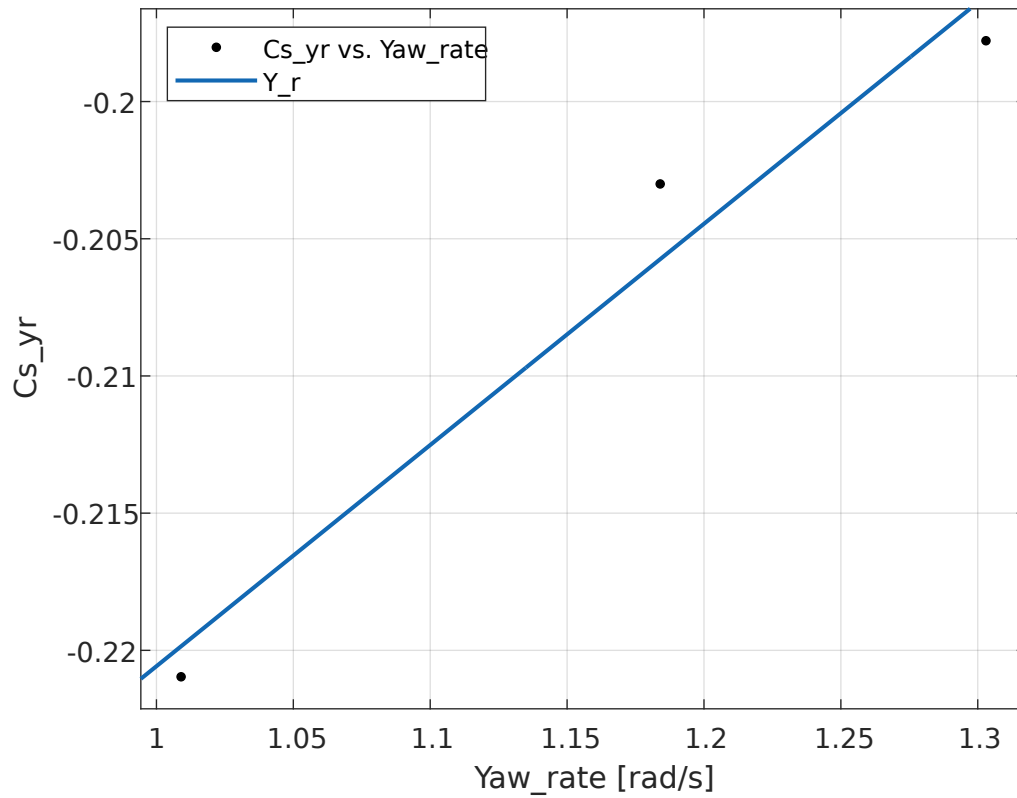


Figure 6.11: Y_r

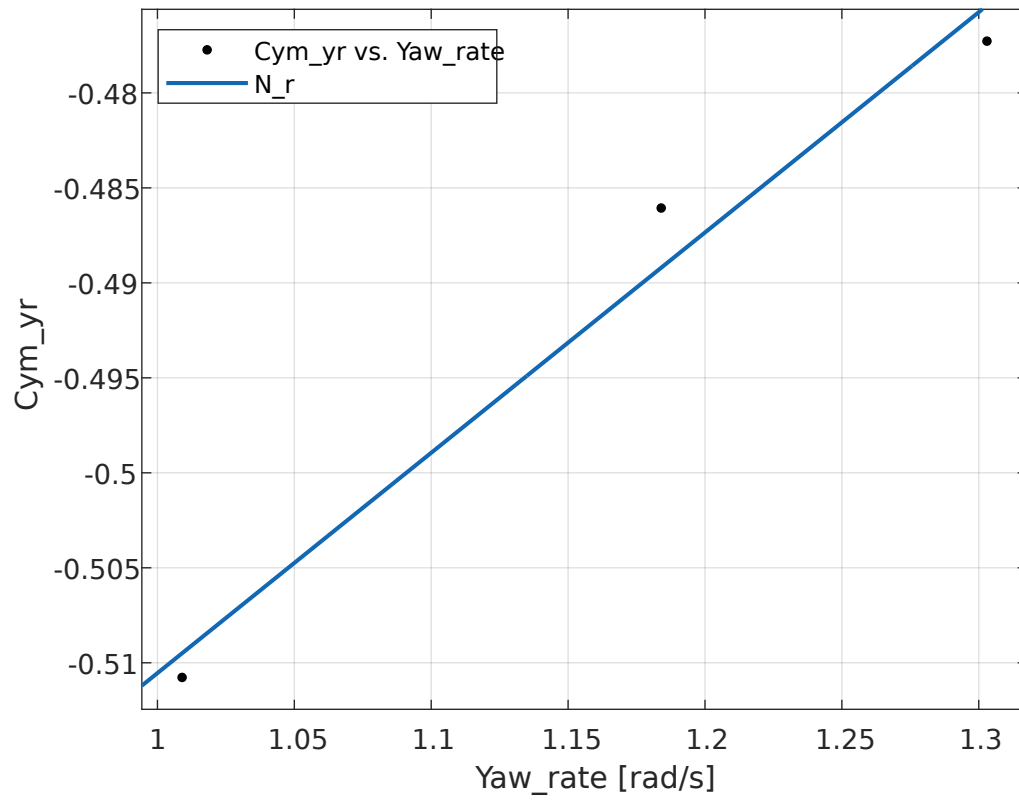


Figure 6.12: N_r

6.5 Beta Simulation

In this section, I will show the results of simulations as the sideslip angle changes. For these simulations, a calculation domain has been adopted that is identical to the simulations in the straight ahead and the simulations at varying pitch angle. The sideslip angles used for these simulations are angles between 0 and 10 degrees. The coefficients evaluated are the side force coefficient C_s and the moment coefficient around the z-axis C_{YM} .

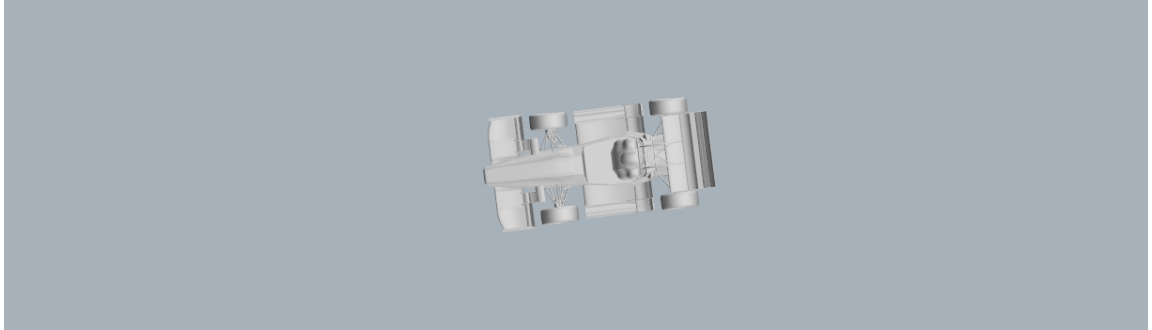


Figure 6.13: Sideslip Simulation - Top View

Once all simulations were performed and the coefficients derived, the focus was on where the variation of the coefficients was in the linear range. In this range of angles, the derivation of the aerodynamic coefficients of interest was carried out. In this way the aerodynamics derivatives Y_β and N_β has been calculated as a proportionality coefficient of the side force and yaw moment coefficient against sideslip. The constant terms $C_{s,\beta}$ and $C_{YM,\beta}$ has been calculated as constant term from these CFD analyses.

From the CFD simulations the following table has been obtained:

Sideslip Angle β [deg]	C_z	C_s	C_{YM}
1	-4.76	-0.0009	0.078
2	-4.74	-0.0262	0.006
3	-4.66	-0.0503	0.002
5	-4.53	-0.1142	-0.037
7	-4.00	-0.1837	-0.091
10	-3.41	-0.3407	-0.238

Table 6.3: Sideslip Table Coefficient

Thanks to the "Curve Fitting" tool of Matlab a linear regression was calculated and the following results were derived :

- $Y_{\beta} = -0.03709 [1/deg]$
- $N_{\beta} = -0.03141 [1/deg]$
- $C_{s,\beta} = 0.05377$
- $C_{YM,\beta} = 0.09976$

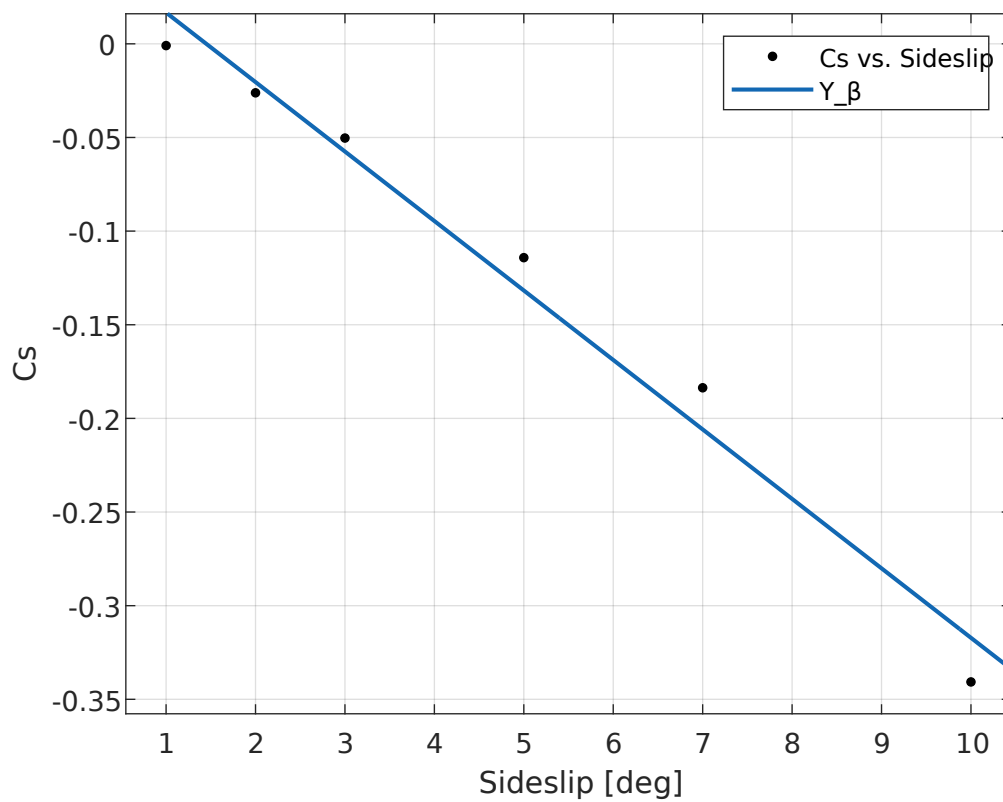


Figure 6.14: Y_{β}

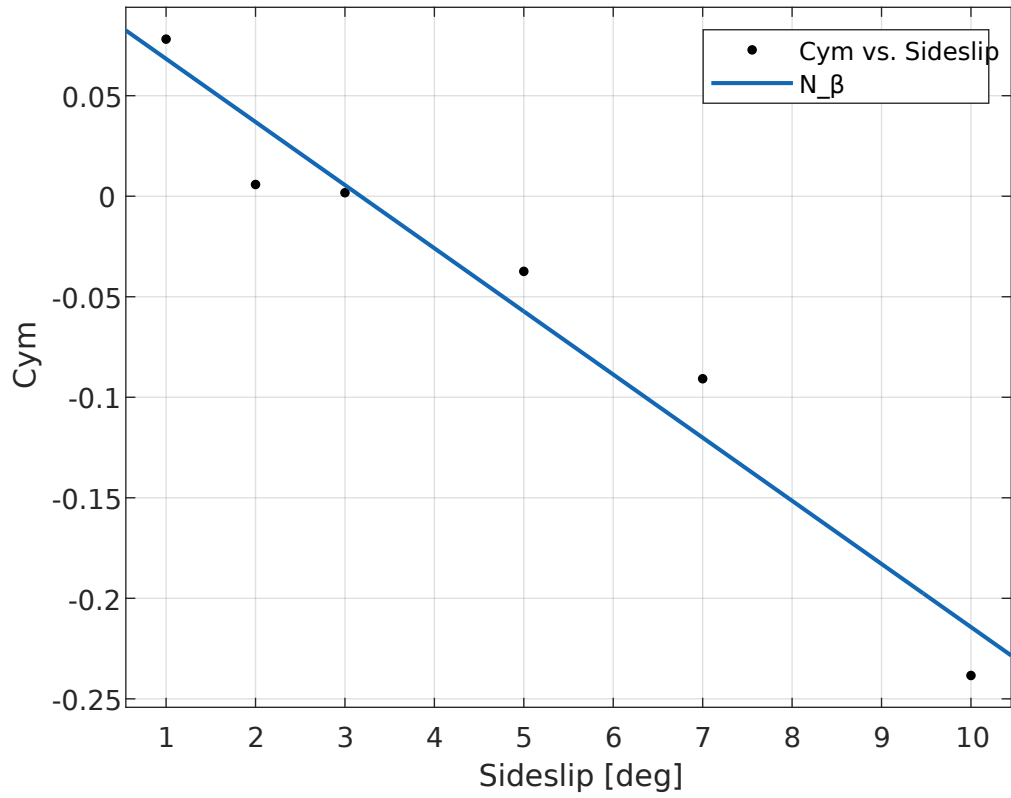


Figure 6.15: N_β

6.6 Results

	Y_r [s/rad]	Y_β [1/deg]	$C_{s,0}$
C_s	0.08062	-0.03709	-0.24743

Table 6.4: Sideforce Aerodynamics Coefficient Derivatives

	N_r [s/rad]	N_β [1/deg]	$C_{YM,0}$
C_{YM}	0.116	-0.03141	-0.52674

Table 6.5: Yaw Moment Aerodynamics Coefficient Derivatives

The values $C_{s,0}$ and $C_{YM,0}$ were obtained from the sum of the constant terms of the aerodynamic derivatives of the sideforce and yaw moment coefficients of the sideslip and yaw rate simulations.

To verify the accuracy of the linear model, a comparison was made with a skidpad simulation carried out using data from the Varano race logs.

The simulation data are as follows:

- speed = 34 km/h
- radius = 9.38 m
- $\beta = 1.98$ deg
- rollio = 0.71 deg

With 34 km/h value of velocity and 9.38 m value of curve radius you have a yaw rate value of about 1.009.

This table compares the results from the simulation and those obtained with the linear model

	C_s	C_{YM}
CFD	-0.26	-0.51
Linear Model	-0.24	-0.47

Table 6.6: Comparison of CFD and Linear Model

As can be clearly seen from the table, the model closely approximates the results obtained from the simulation. The discrepancy between the two results may be due to the fact that the Skidpad simulation model also includes the roll angle, which influences the aerodynamic behavior of the vehicle.

This linear model performs exceptionally well for Formula SAE cars due to their relatively high yaw rates. However, it may not be as suitable for other Formula cars that exhibit lower yaw rates. In such cases, it is often more advantageous to rely on pure sideslip simulations.

Additionally, it's worth noting that even for Formula SAE cars, during the initial phases of a curve, it is more advantageous to exclusively employ the sideslip model. This is because the contribution of the yaw rate component is less significant during these moments. In fact, simulations involving lower yaw rate values exhibit a distinct and less pertinent trend.

Hence, for the initial stages of a curve, the sideslip model alone proves to be a more effective choice.

Chapter 7

Conclusion and Future Work

7.1 Summary of Findings

In this thesis, we embarked on a comprehensive journey to validate a Computational Fluid Dynamics (CFD) model for Formula SAE vehicles within the controlled environment of a wind tunnel. The primary objective was to assess the model's capability to accurately simulate the aerodynamic performance of the vehicle, focusing on key parameters such as the aerodynamic coefficients, pressure distributions, and wake measurements. Through meticulous analysis and rigorous experimentation, we have successfully achieved the goal of validating the CFD model.

The analysis of the aerodynamic coefficients played a pivotal role in evaluating the accuracy of our CFD model. By comparing the CFD-predicted values to the experimental results obtained in the wind tunnel, we were able to ascertain the model's ability to reproduce the real-world behavior of the Formula SAE vehicle. The close agreement between the simulated and measured values for coefficients such as lift, drag, and downforce is a testament to the model's predictive power.

Moreover, our investigation extended beyond mere surface pressure distributions, delving into the realm of pressure coefficients. The data obtained from pressure coefficient measurements on the vehicle's rear section were critical in affirming the model's credibility. The model not only replicated the pressure coefficients accurately but also demonstrated its ability to capture the subtle variations and gradients crucial for understanding the complex aerodynamic interactions taking place on the rear of the vehicle.

Perhaps the most compelling evidence of the CFD model's validity emerged from our examination of wake measurements. The wake of a Formula SAE vehicle plays a vital role in determining its overall aerodynamic performance and stability. The

model's capacity to replicate wake flow patterns, vortex shedding, and turbulence characteristics was strikingly similar to the experimental observations in the wind tunnel. This alignment between simulation and reality underscores the model's efficacy in capturing the intricacies of vehicle aerodynamics.

In conclusion, our extensive validation process has convincingly demonstrated that the CFD model for the Formula SAE vehicle used in this study is robust and dependable. The close agreement between CFD predictions and wind tunnel measurements for aerodynamic coefficients, pressure coefficients, and wake characteristics attests to the model's capability to faithfully reproduce the real-world aerodynamic behavior of the vehicle. As such, it can be confidently asserted that the CFD model is validated and can serve as a valuable tool for future aerodynamic studies, design optimizations, and performance evaluations of Formula SAE vehicles.

With the CFD model validated, it was possible to move on to the second part of the thesis: derive the aerodynamic coefficients of an SAE Formula car under curve conditions. By developing a linear model that decomposes the cornering moment into its yaw and sideslip components, we have laid the foundation for a deeper understanding of the complex aerodynamic forces at play during high-speed cornering.

Extensive literature review, data collection, and meticulous mathematical analysis were conducted to formulate the proposed model. This research effort has deepened our understanding of the intricate aerodynamic forces that influence the behavior of SAE Formula cars during curve negotiation.

A significant contribution of this research is the development of a dependable model that accurately characterizes aerodynamic coefficients under curve conditions. The model's ability to separate the cornering moment into yaw and sideslip components enhances our comprehension of the underlying physical phenomena and holds promise for applications in vehicle design and control systems. Moreover, the derived aerodynamic coefficients allow for the construction of aerodynamic maps that encompass cornering situations. These maps serve as valuable tools for engineers and designers, facilitating the prediction and optimization of a vehicle's performance during high-speed cornering maneuvers. Such optimization can have a profound impact on aspects like vehicle stability, suspension tuning, and overall lap times.

To summarize, this thesis has successfully fulfilled its objectives by presenting a robust linear model for the derivation of aerodynamic coefficients in the context of SAE Formula cars operating under curve conditions.

7.2 Future Recommendations

For more accurate validation of the CFD model in future experiments, it is essential to refine the vehicle setup in the wind tunnel. This entails meticulous attention to detail during the preparation of the test vehicle. Specifically, greater care should be taken in configuring the vehicle's parameters, ensuring that they are precisely aligned with the intended conditions. One critical aspect to address is the precise measurement and adjustment of ground clearances. This information should be known a priori to eliminate any uncertainties associated with ride height variations during testing. Such improvements in setup will contribute significantly to the reliability and consistency of the experimental results.

Mesh quality plays a pivotal role in the accuracy of CFD simulations. To further refine our CFD model, we suggest exploring advanced meshing techniques. Specifically, one promising avenue is to experiment with volumetric meshing using software such as BETA CAE ANSA. Volumetric meshing offers advantages in terms of resolving complex geometries and boundary layers more accurately. By adopting this approach, we can potentially achieve higher fidelity in our simulations and improve our understanding of the aerodynamic behavior of the vehicle.

Bibliography

- [1] Pictures at Hockenheimring, <https://www.formulastudent.de/pr/pictures/> (cit. on p. 2).
- [2] John D. Anderson. *Computational Fluid Dynamics*. Ed. by McGraw-Hill. First. Inc., USA: McGraw-Hill, 1992 (cit. on p. 7).
- [3] Notes from Lecture 'Car Body Design and Aerodynamics', Professor A.Tonoli (cit. on p. 12).
- [4] Turbulence Modeling in CFD simulations, <https://cfdflowengineering.com/turbulence-modeling-in-cfd-simulations/> (cit. on p. 15).
- [5] Note from Lecture 'Design of Engine and Control System - Charge Motion Within The Cylinder', Professor E.Spessa (cit. on p. 15).
- [6] Milovan Perić Joel H. Ferziger. *Computational Methods for Fluid Dynamics*. Ed. by Springer. 3rd. Germany: Springer, 1996 (cit. on p. 16).
- [7] External Aerodynamics with Simcenter STAR-CCM+ 'Guidelines for FSAE cars', Claudio Santarelli, Léon Reketat (cit. on p. 19).
- [8] Determination of CFD domain sizing for FSAE car cornering case, Siemens (cit. on p. 57).
- [9] Developing Steady-State Cornering CFD, Maurice Nayman, Chris Penny (cit. on p. 58).
- [10] Aerodynamics Evaluation of Road Vehicles in Dynamic Maneuvering, SAE International (cit. on p. 59).